



DESN2000

Engineering Design and Professional Practice

Final Report

H14A: Team 1

Catherine Cheng	z5310517@unsw.edu.au	z5310517
Courtney Coates	z5175357@unsw.edu.au	z5175357
Dan Nguyen	z5206032@unsw.edu.au	z5206032
James Jiang	z5206109@unsw.edu.au	z5206109
Melissa Thein	z5361928@unsw.edu.au	z5361928
Nikki Fang	z5310518@unsw.edu.au	z5310518

2022/11/27

Executive summary

Sensor-based safety monitoring is known to be the leading factor in reducing the risk of air-quality related illness and death; however, operation and maintenance remains costly and environmentally detrimental. In a climate of ever-increasing urban city environmental impact, the need for environment-neutral urban safety systems is rising.

A solution is proposed to harvest the energy of air conditioning exhaust in urban buildings to power a sensor-based monitoring system.

Research shows that air-conditioning use in urban buildings is large, accounting for 1/5 of daily energy consumption. Central vent systems in these buildings have substantial volumes of air flow for upwards of 12 hours per day, creating an opportunity for a turbine-based energy harvesting system.

A two-bladed Savonius vertical axis wind turbine was found to be the most suitable air harvester in the environment of low velocity air flow. A twisted dual blade design provides a large surface area, generating high levels of torque. Multi-directional functionality allows for maximum use of vent air flow. Encased in an innovative aerodynamic fairing, total generated power exceeds 5 watts.

A modular approach was taken for the connection of safety monitoring systems, maximising accessibility and adaptability. Battery energy storage allows for interchangeable sensor connections through embedded USB-C ports. An IoT device is included for instant streaming and notification systems, furthering the safety monitoring capabilities of the solution.

Axiomatic design theory and functional concept coupling was used for design feasibility and technical solution choices. All solution aspects were designed within constraints of the outlined budget, Australian safety regulations, and specific air vent height and weight regulations.

Team statement

The contribution of each team member to this report is summarised here. The team has worked well together over the term and is very proud to have completed this report.

Catherine:

- Preliminary design concept literature review.
- Axiomatic design matrices and functional coupling analysis.
- Aerodynamic fairing calculations.
- 2D component drawings.

Courtney:

- Executive summary.
- Battery & IoT selection and charging process.
- Design constraints.
- Writing consistency, proofread, and final edit of report.

Dan:

- Technical design methodology.
- Mechatronic system design: power requirements.
- Designing for assembly.
- FEA optimisation process.
- Spline design.
- Circlip selection.
- Turbine blade optimisation.
- Bearing selection.
- Vent interface.
- CAD model.
- Technical analysis of wind energy within air vents.
- Factor of safety.

James:

- Feasibility study.
- Mechatronic system design: generator selection.
- Aerodynamic fairing.
- Vertical turbine type.
- Turbine blade.
- Turbine power output.
- Drive train.
- Prototype and 3D-printing.
- General L^AT_EX formatting and table styling.
- Biography headshots for everyone.

Melissa:

- Introduction.
- Bolt selection.
- Conclusion.

Nikki:

- Customer needs and functional requirements.
- Design concept sketches.
- 2D component drawings.
- Assembly drawing and bill of materials.

Contents

1	Introduction	1
2	Reflection on conceptual design	2
2.1	Conceptual design process	2
2.2	Customer needs	2
2.3	Functional requirements	3
2.4	Preliminary design concepts: horizontal axis wind turbine	4
2.5	Preliminary design concepts: bladeless turbine	5
2.6	Preliminary design concepts: vertical axis turbine	6
2.7	Axiomatic design theory	7
2.8	Functional coupling of the horizontal axis turbine	8
2.9	Functional coupling of the bladeless turbine	9
2.10	Functional coupling of the vertical axis turbine	10
2.11	Final design choice	11
3	Technical design methodology	11
4	Technical design and analysis: Power	12
4.1	Feasibility study	12
4.2	Mechatronic system	12
4.3	Aerodynamic fairing	14
4.4	Vertical turbine type	14
4.5	Turbine blade	16
4.6	Turbine power output	17

4.7	Drive train	18
5	Technical design and analysis: Fasteners	19
5.1	Designing for assembly	19
5.2	FEA optimisation process	19
5.3	Spline design	20
5.4	Circlip selection	23
5.5	Turbine blade optimisation	23
5.6	Bearing selection	24
5.7	Bolt selection	26
5.8	Vent interface	27
6	CAD model	28
7	Conclusion	39

References

Biography

- A Technical analysis of wind energy within air vents**
- B Battery life**
- C Mechatronic system power**
- D Technical analysis and selection of the electric generator**
- E Technical design and analysis of the aerodynamic fairing**
- F Change in fluid power**

G Flettner ventilator

H Technical analysis of turbine output power

I Technical analysis and design of the drive train

J Factor of safety

K Finite element analysis of axial spline loads

L Finite element analysis of rotational spline loads

M Circlip calculation

N Finite element analysis for blade optimisation

O Bearing selection

P Bolt selection

Q Slipping calculation

R Tipping calculation

S Three-quarter CAD render

T Detailed bill of materials

U Prototype

1 Introduction

Global urbanisation has significantly changed the way people live and work; over half of today's population living in dense, environmentally-concerning cities [1]. More than 80% of people living in urban areas are exposed to air pollution levels that exceed World Health Organisation guidelines [2]. In particular, the working class are subject to additional airborne hazards, with poor air quality being responsible for 450,000 deaths in the workplace between 2000-2016 [3]. Therefore, it is crucial to design and implement systems to rigorously monitor air quality and reduce the risk for the estimated 545 million people [4] worldwide who suffer from existing chronic respiratory conditions.

In the interim presentation, thorough research was performed to gain insights into the advantages and disadvantages of existing solutions. Additionally, an online survey of 97 people was conducted to learn about potential users' stories and their needs. This enabled the initial ideation of ways to address the issue.

This report contains 3 main sections which detail the progress made since the interim presentation: Reflection on conceptual design, Technical design and analysis, and CAD modelling. Within the reflection on conceptual design, further research into turbine designs was considered carefully alongside customer needs to generate preliminary design solutions, which were evaluated using axiomatic design theory. Aiming to minimise coupling, the InVent system was optimised, utilising a vertical axis wind turbine to harvest the energy of air-conditioning exhaust to power a sensor-based air quality monitoring system. Technical design and analysis demonstrates valid calculations used to determine the harvesting capabilities of air inside vents, the estimated power output, and the system's power requirements. Turbine, blade, fastener, and generator selections are justified. Fastener analysis and power transmission analysis are focused on to design the most suitable system. Finally, a CAD model of the InVent system was developed, including a 3D model of the final design concept, assembly drawings with an exploded view, bill of materials and 2D drawings of each component.

2 Reflection on conceptual design

2.1 Conceptual design process

The conceptual design process consisted of extensive market research including a survey of 97 people to generate a problem statement, user stories, and the derivation of customer needs and functional requirements. These steps in the design process were discussed in detail in the interim and final design presentations but are reiterated briefly below. Finally, the functional requirements were used to generate three preliminary design concepts which were then evaluated using Axiomatic Design Theory.

2.2 Customer needs

The customer needs shown in Table 1 were devised to reflect customer expectations for the energy harvesting device.

Table 1: Customer needs.

Customer needs		Description
CN(1)	Safe working environment	Companies should be able to identify air quality issues and be compliant with the NSW Public Health Act.
CN(2)	Air quality measuring	The device should be able to measure air quality and detect air quality issues.
CN(3)	Constant monitoring	Air quality data should be available constantly.
CN(4)	Low energy consumption	Should be efficient and harvest wasted energy.
CN(5)	Non-disruptive	Should not disturb current lifestyle of residents or inconvenience them.
CN(6)	Adaptable to infrastructure	Ensure device can fit into a range of different buildings.

2.3 Functional requirements

The functional requirements were formulated by translating the previously identified customer needs into fundamental behaviours the design must have. The primary functional requirement is to monitor the air quality of workplaces, which can be decomposed into several sub-level functional requirements. These were further decomposed where possible, and finally, a range of target values was specified for functional requirements in the lowest level. The devised functional hierarchy is shown in Figure 1.

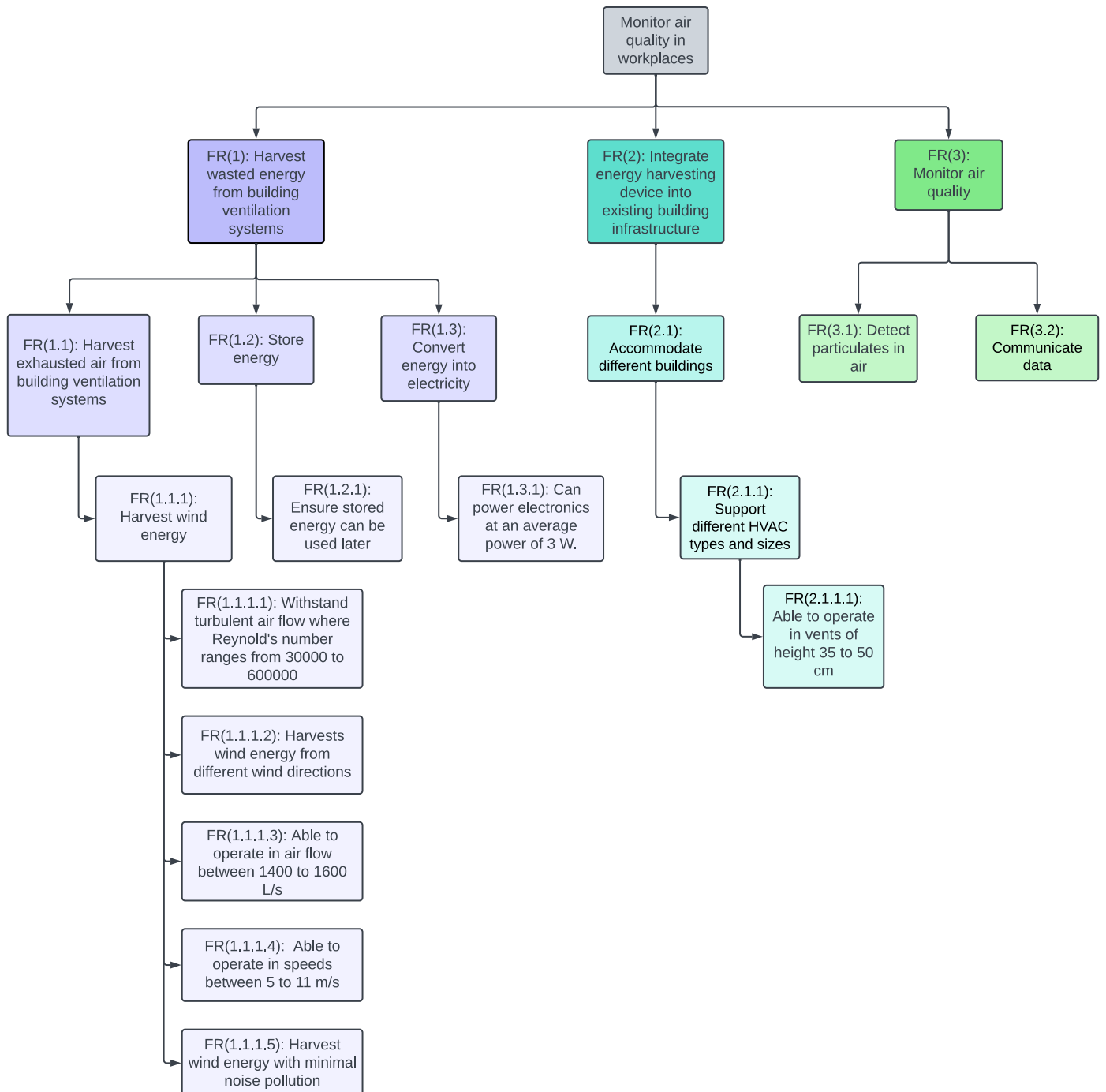


Figure 1: Functional requirements hierarchy.

Table 2 summarises the functional requirements in the lowest level of the hierarchy and indicates the customer needs satisfied by each one.

Table 2: FR breakdown.

Functional requirements	Customer needs satisfied
FR(1.1.1.1): Withstand turbulent air flow where Reynold's number ranges from 30000 to 600000.	CN(6)
FR(1.1.1.2): Harvests wind energy from different wind directions.	CN(4), CN(6)
FR(1.1.1.3): Able to operate in air flow between 1400 to 1600 L/s.	CN(6)
FR(1.1.1.4): Able to operate in speeds between 5 to 11 m/s.	CN(6)
FR(1.1.1.5): Harvest wind energy with minimal noise pollution.	CN(5)
FR(1.2.1): Ensure stored energy can be used later.	CN(3), CN(4)
FR(1.3.1): Can power electronics at an average power draw of 3 watts.	CN(2), CN(3)
FR(2.1.1.1): Able to operate in vents of height 35 to 50 cm.	CN(6)
FR(3.1): Detect particulates in air.	CN(1), CN(2)
FR(3.2): Communicate data.	CN(1), CN(2)

2.4 Preliminary design concepts: horizontal axis wind turbine

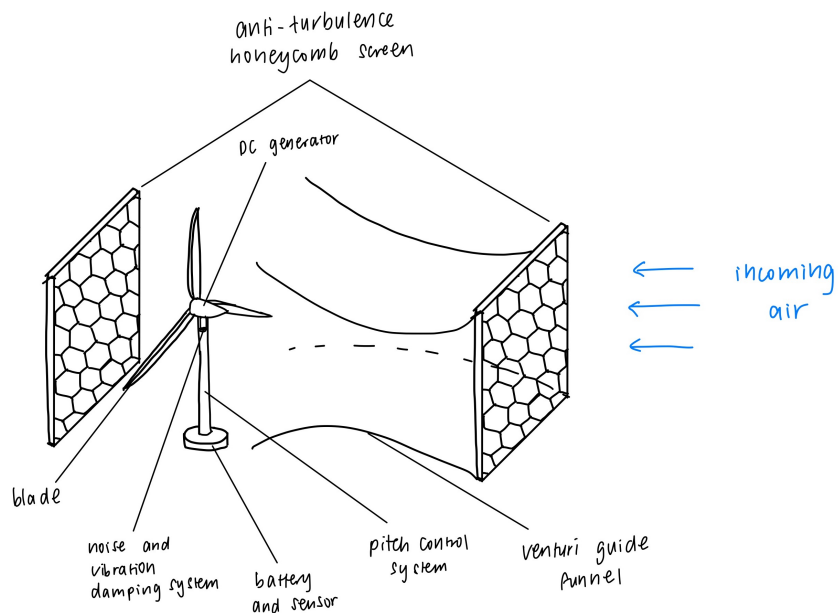


Figure 2: Annotated sketch of horizontal axis wind turbine concept.

The horizontal axis wind turbine (HAWT) concept originates from the classic 3-blade wind turbine, scaled down to fit comfortably inside ventilation ducts. HAWTs perform best in low turbulent airflow with consistent wind direction [5]. As such, the design includes anti-turbulence honeycomb screens (which has seen experimental success in turbulent wind tunnels [6]) to reduce turbulence of incoming flow. A pitch control system is used for adjusting the turbine to respond to changes in airflow direction in the duct. A venturi inlet guide funnel is installed at the intake of the turbine to accelerate oncoming wind.

To reduce noise pollution from outgoing turbulence, a vibration dampening system is installed at the base of the turbine, where the unit interfaces with the vent. An anti-turbulence honeycomb screen is also installed downwind to reduce the turbulence of the wake, consequently reducing noise.

The turbine blades turn along a horizontal axis, actuating a DC generator. The swept area of the turbine blades is directly proportional to the power generated [7]. The turbine blade length is maximised as this increases swept area, and works better in areas of lower wind speed [8]. The design has 2 blades to maximise efficiency and reduce wind resistance, making it more suitable for low air speeds [7]. The generated electrical energy is stored in a battery, which powers the sensor and an Internet of Things (IoT) data transmitter.

2.5 Preliminary design concepts: bladeless turbine

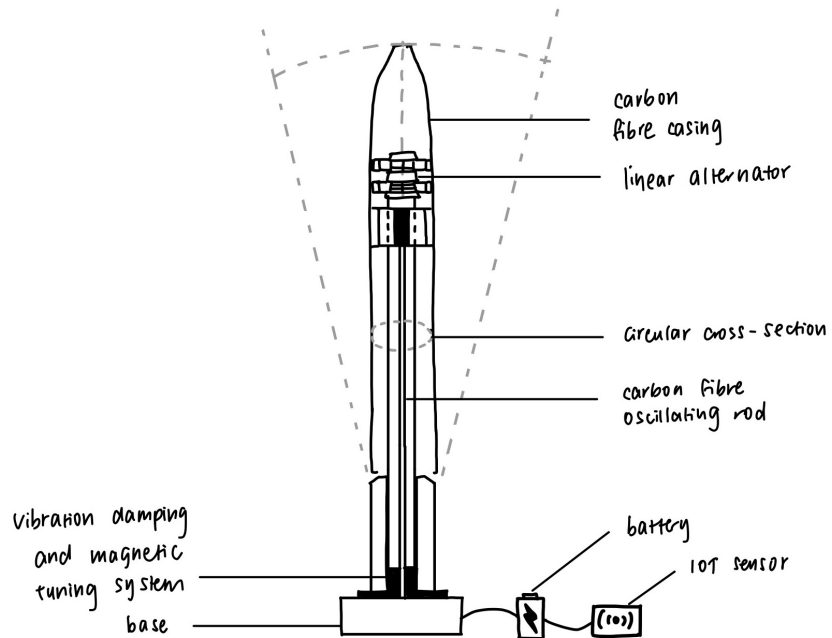


Figure 3: Annotated sketch of Bladeless turbine concept.

The bladeless turbine concept harvests energy from turbulent airflow phenomena, known as vortex shedding [9]. The turbine body has a circular cross sectional area, ensuring perpendicular incident air regardless of airflow direction [10], which is necessary for the ever changing airflow direction inside ventilation ducts. The bottom of the turbine is anchored to the vent with a vibration dampening system to reduce unwanted noise pollution, whilst the tip is free to oscillate. As a result, the body material needs to be strong and lightweight, making carbon fibre a suitable choice [11]. The air induces vibration in the turbine body which, within a certain velocity range, causes the turbine rod to oscillate at its natural resonance frequency. The velocity range is widened using a magnetic tuning system [10]. The kinetic vibration is converted into electricity using a linear alternator system [10]. The electrical energy is stored in a battery, which powers the sensor and an IoT data transmitter.

2.6 Preliminary design concepts: vertical axis turbine

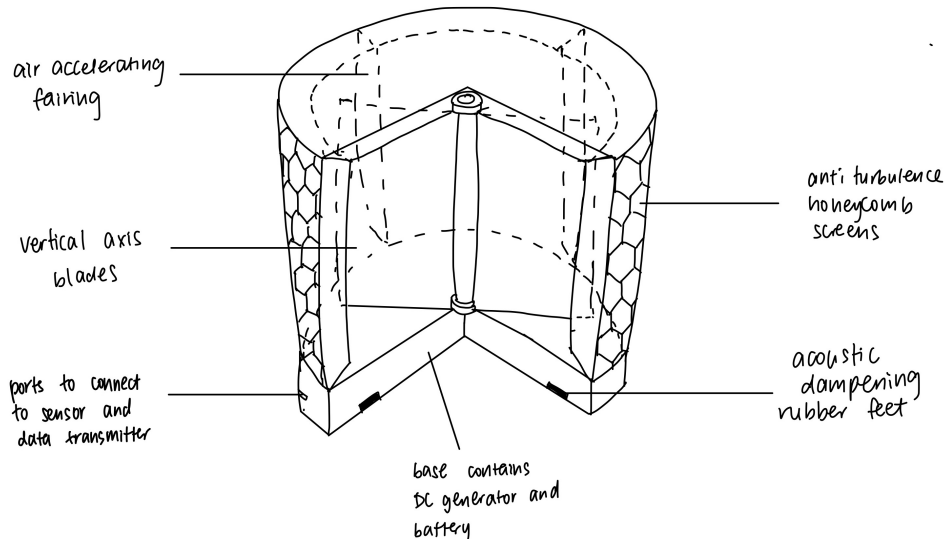


Figure 4: Annotated sketch of vertical axis turbine concept.

The vertical axis wind turbine captures wind from multiple directions, necessary for the ever changing airflow direction inside ventilation ducts. The turbine is encased by a fairing that accelerates the oncoming air before it reaches the blades by decreasing the cross sectional area of the flow. At each of the air inlets, a honeycomb screen reduces the incoming turbulence of the air, and ensures that wind energy can be harvested in any turbulent environment. At the base of the turbine are rubber feet designed to dampen acoustic noise and vibration generated by the turbine. The turbine is packaged in a compact design that will easily fit inside typical duct sizes of around 500 mm by 500 mm, making it suitable for everything from industrial kitchen vents to residential building ducts.

2.7 Axiomatic design theory

Axiomatic design theory, and more specifically the independence axiom, states that a design should maintain independence between the functional requirements and the design parameters of a system. In other words, a design is deemed to be coupled if changing a design parameter will result in effects on separate functional requirements.

This philosophy helped guide the conceptual design process by helping refine each design concept so that all FRs would be met, as well as reducing the impact of coupling on the final design. FR-DP matrices were constructed in order to analyse FR independence.

The functional requirements referenced in the FR-DP matrices in the following subsections were derived from the lowest level of the functional hierarchy generated earlier:

- FR (1.1.1.1): Withstand turbulent airflow where Reynold's number ranges between 30,000 - 600,000.
- FR (1.1.1.2): Harvests wind energy from different wind directions.
- FR (1.1.1.3): Able to operate in airflow between 1400 - 1600 L/s.
- FR (1.1.1.4): Able to operate between 5 - 11 m/s.
- FR (1.1.1.5): Harvest wind energy with minimal noise pollution.
- FR (1.2.1): Ensure stored energy can be used later.
- FR (1.3.1): Harvest enough electricity to power a device (500 - 800 mW).
- FR (2.1.2.1): Able to operate in vents of height 50 cm.
- FR (3.1): Detect particulates in air.
- FR (3.2): Communicate data.

Design parameters, including components, features, systems and processes were then identified in each preliminary design concept, and matched with the above FRs.

This was instrumental in helping identify functional requirements not yet met by each concept, which then led to refining of the original concepts, informed by the axiomatic design process. Coupling present between FRs and DPs in the original designs was also identified, and where possible, DPs were varied to better align with the independence axiom.

2.8 Functional coupling of the horizontal axis turbine

These were the design parameters identified for the horizontal axis turbine design:

- DP (1): Anti-turbulence honeycomb screens.
- DP (2): Pitch control system.
- DP (3): 3 blade design.
- DP (4): Venturi inlet guide funnel.
- DP (5): Noise and Vibration dampening system.
- DP (6): Battery.
- DP (7): DC generator.
- DP (8): 15 cm length blades.
- DP (9): Sensor.
- DP (10): IoT data transmitter.

Table 3: FR-DP matrix for horizontal turbines.

		DP									
		1	2	3	4	5	6	7	8	9	10
FR	1.1.1.1	×									
	1.1.1.2		×								
	1.1.1.3			×					×		
	1.1.1.4			×	×				×		
	1.1.1.5					×					
	1.2.1						×				
	1.3.1		×	×				×			
	2.1.2.1								×		
	3.1									×	
	3.2										×

From Table 3, it is evident that the horizontal axis turbine is unable to satisfy the independence axiom. Some design parameters are addressing multiple functional requirements, implying that the product architecture is not optimised. For example, DP (2) (pitch control system) addresses FR (1.1.1.2) (harvests wind energy from different wind directions) and FR (1.3.1) (harvest enough electricity to power a device). Without a pitch control system, the turbine is not optimised for multi directional flow, and hence not enough power can be generated to power the sensors.

Thus, it can be concluded that the horizontal axis turbine is a decoupled design concept, and hence not the most suitable design direction.

2.9 Functional coupling of the bladeless turbine

The design parameters identified in the bladeless turbine design are:

- DP (1): Circular cross sectional area.
- DP (2): Oscillating rod of height 25 cm.
- DP (3): Magnetic tuning system.
- DP (4): Vibration dampening system.
- DP (5): Battery.
- DP (6): Linear alternator system.
- DP (7): 30 cm carbon fibre casing.
- DP (8): Air quality sensor.
- DP (9): IoT data transmitter.

Table 4: FR-DP matrix for bladeless turbines.

		DP								
		1	2	3	4	5	6	7	8	9
FR	1.1.1.2	×								
	1.1.1.3		×	×						
	1.1.1.4		×	×						
	1.1.1.5				×					
	1.2.1					×				
	1.3.1						×			
	2.1.2.1		×					×		
	3.1								×	
	3.2									×

Note that several functional requirements were deemed irrelevant for this particular design and were therefore not included in the matrix. Notably, FR (1.1.1.1) (Withstand turbulent airflow) was omitted since the innate function of bladeless turbines is to harness energy from turbulent airflow.

From Table 4, it can be concluded that the bladeless turbine design is fairly uncoupled. Almost all design parameters address a single functional requirement, satisfying the independence axiom. The notable exception is DP (2) (Oscillating rod of height 25 cm), which addresses FR (1.1.1.3) (Able to operate in airflow between 1400 - 1600 L/s), FR (1.1.1.4) (Able to operate between 5 - 11 m/s) and FR (2.1.2.1) (Able to operate in vents of height 35 - 50 cm).

Since the design is uncoupled, it is a suitable design for consideration.

2.10 Functional coupling of the vertical axis turbine

These are the design parameters identified in the vertical axis design:

- DP (1): Anti-turbulence honeycomb screen on inlet areas.
- DP (2): Turbine axis perpendicular to airflow.
- DP (3): Large turbine blade swept volume of 5.5L.
- DP (4): Air accelerating fairing.
- DP (5): Rubber dampening feet.
- DP (6): Battery.
- DP (7): DC generator.
- DP (8): Fairing height of 25 cm.
- DP (9): Sensor.
- DP (10): IoT data transmitter.

Table 5: FR-DP matrix for vertical axis turbines.

		DP									
		1	2	3	4	5	6	7	8	9	10
FR	1.1.1.1	×									
	1.1.1.2		×								
	1.1.1.3			×							
	1.1.1.4				×						
	1.1.1.5					×					
	1.2.1						×				
	1.3.1				×			×			
	2.1.2.1								×		
	3.1									×	
	3.2										×

From Table 5, it is evident that the vertical axis turbine design is uncoupled. Again, almost all design parameters address a single functional requirement, satisfying the independence axiom. The notable exception is DP (4) (air accelerating fairing), which addresses both FR (1.1.1.4) (able to operate between 5 - 11 m/s) and FR (1.3.1) (harvest enough electricity to power a device) since the fairing ensures the flow is accelerated to speeds necessary to generate sufficient power.

2.11 Final design choice

Ultimately, axiomatic design theory played a pivotal role in the decision making process for the final design direction of the product. This method made it apparent that the horizontal axis wind turbine design exhibited significant functional coupling, and was therefore not the best product option. Analysis of the bladeless turbine and vertical axis turbine revealed both as viable design options, characterised by low functional coupling. It was evident that the vertical axis turbine was the most uncoupled design out of the three options, and that this design exhibited the most independence between functional requirements and design parameters. The generated matrix for the vertical axis turbine highlighted its capacity to address each of the necessary functional requirements while simultaneously minimising the negative implications of coupling on design. For these reasons, the decision to design a vertical axis wind turbine was made.

3 Technical design methodology

With consideration of the functional requirements outlined in Table 2, the technical design methodology of the turbine is as follows:

1. Feasibility study of the wind energy to confirm how much power can be extracted from the air duct;
2. Design of the mechatronic system to identify power requirements to power the sensors and IoT;
3. Design of the aerodynamic fairing to increase the air velocity appropriately to the turbine's operating requirements;
4. Selecting and calculating the power yield of a vertical turbine type and turbine blade type;
5. Design of a drive train to match the power yield of the turbine to the peak RPM performance of the generator; and,
6. Designing parts and fastening techniques with a finite-element analysis (FEA) optimisation process.

4 Technical design and analysis: Power

4.1 Feasibility study

A feasibility study is performed to determine the power of fluid obtainable from the airflow of a range of ventilation ducts at the minimum air velocity of 5 m/s (Appendix A). The power of fluid equation (Equation 4), derived from the kinetic energy equation, is used to calculate the power of the airflow through a given cross-sectional area. The calculated power is then multiplied by Betz's coefficient, 16/27, since Betz's Law states only 59.3 % of the kinetic energy of the fluid can be converted to usable mechanical energy by an ideal turbine [12]. Table 18 shows the maximum obtainable power by an ideal turbine which (by inspection) validates the feasibility of the turbine-based concept to power a small mechatronic system.

4.2 Mechatronic system

As the application of the turbine is to power sensors, the mechatronic system is designed to place additional power constraints for turbine design. Assume the mechatronic system contains the following table of devices in Table 6.

Table 6: Power rating of mechatronic system devices.

Device	Description	Input Voltage (V)	Input Current (mA)
Arduino UNO	Micro-controller.	7 - 20	50 - 200
Arduino WiFi Shield	WiFi module.	5	150
DHT11	Temperature and humidity sensor.	5	2.5
MICS6814	Gas sensor	5	32
SPS30	Particulate matter sensor.	5	16
BME680	Air quality sensor.	5	20

From the power ratings of Table 6, the mechatronic system in Figure 5 is modelled as an interface diagram showing the power and data interfaces.

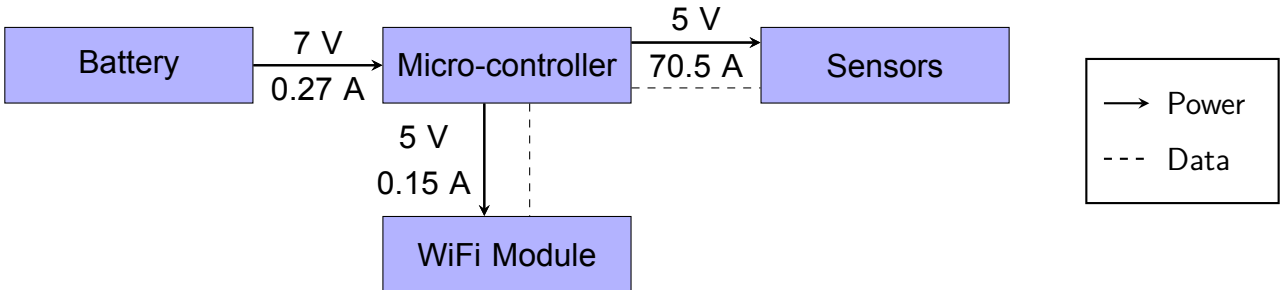


Figure 5: Mechatronic system interface diagram.

From Figure 5, the battery requires a supply voltage of at least 7 V and a supply current of at least 0.27 A. The desired battery capacity was calculated from the battery life formula (Equation 5) as 1.8 Ahr thus yielding an average battery life of 6.66 hr (refer to Appendix B for a full calculation).

The power consumption of the mechatronic system with only the essential devices enabled i.e. the Arduino UNO and Arduino WiFi Shield requires a voltage of at least 7 V and current of 0.2 A. The power consumption was calculated from the electrical power formula (Equation 6) as 1.4 W (refer to Appendix C for a full calculation).

From the power requirements, a suitable generator was selected to convert the mechanical energy of the turbine to electrical energy. Due to the traditionally low rotational speed of turbines, it was crucial to select a generator that could provide adequate power at a low RPM. The generator also had to be compact and small in size as to fit within the base of the device.

It is possible to use motors as electric generators [13]. Therefore, for this scale it was determined that motor-generators were best suited for electricity production.

As seen in Figure 15 of Appendix D, the operating window of the stepper motor is significantly lower. Therefore, a compact stepper motor has been validated to be most suitable for electric generation for this situation [14]. The NEMA-11 stepper motor was chosen as it has been proven to generate electricity reliably [15].

It has been resolved in Appendix D that ~1100 RPM is required to produce an electric output of ~5 W. This will satisfy the minimum power requirements of the mechatronic system (1.4 W), and allow the addition of multiple sensor devices as per customer needs.

The electrical circuit in Figure 17 is used to rectify the current and provide a steady voltage to the rest of the electronic systems.

4.3 Aerodynamic fairing

According to Bernoulli's principle [16], when the flow of a fluid is constricted, the velocity of the fluid is increased but at a reduced static pressure in accordance with the Law of conservation of mechanical energy. Therefore, for a constant volumetric flow rate, the air velocity is able to be increased by a factor of 2 by designing the funnel openings (Appendix E) to be of the size shown in Figure 19. This effectively increases the power yield of the turbine as proven in Appendix F.

4.4 Vertical turbine type

There are two main types of vertical turbines that are differentiated by their operating principles. The Darrieus type turbine works by generating lift with aerofoil blades. The Savonius type turbine creates aerodynamic drag with its blades causing it to rotate. Both turbine designs have advantages and disadvantages stemming from their operating principles, and are summarised in Table 7 and Table 8.

While the two types of vertical-axis turbines are not as efficient as horizontal-axis turbines, both can operate independently of wind direction. With the vertical-axis rotor configuration, it allows for the drive train to be packaged within the base of the turbine.

The drag-type Savonius turbine is preferred for this application after qualitative analysis, due to its ability to self-start from low wind speeds and low noise emissions. Savonius turbines are widely used today; one example is the Flettner ventilator, which extracts air by the means of an air scoop that catches air or a breeze. An explosion of the Flettner TXC-2™ ventilator can be seen in Figure 20 of Appendix G.

Operation of the Darrieus design requires a mechanism to start the turbine. This would potentially involve multiple wind sensors for different directions and an added control system to kick-start the rotor once sufficient wind velocity is detected. This adds significant complexity and cost to the proposed device.

As a result of this issue, and a number of other disadvantages shown in Table 7, the decision was made to use a Savonius-derived wind turbine in the design.

Table 7: Advantages and disadvantages of Darrieus wind turbines [17].

Advantages	Disadvantages
Operation is independent of wind direction.	An additional motor is required to start the rotor.
Rotor spins faster than the wind speed.	The angle of attack between the blade and the wind changes throughout its rotation.
	Blades generate peak torque only at two points of the rotation.
	The turbine produces a low amount of torque.
	Large bending moment is created on the rotor as it is not supported at the top.
	High centrifugal stress is exerted on the mechanism by the mass of the rotating mechanism being located far from the rotational axis.
	Turbulent wake produced by the rotor shaft at high wind speeds which affects the trailing blade.

Table 8: Advantages and disadvantages of Savonius wind turbines [18].

Advantages	Disadvantages
Turbine is able to self-start from low wind speeds.	Lower achievable efficiency than other turbine designs.
Low noise emissions.	
Able to operate effectively at low wind speeds.	
Operation is independent of wind direction.	
Higher torque is generated when compared to the Darrieus design.	
Reliable energy conversion can be expected.	

4.5 Turbine blade

The type of Savonius turbine blade design was carefully chosen to yield the most optimal performance under the proposed operating conditions.

In turbine blade design, there is an overarching importance placed upon blade efficiency. The blade efficiency is expressed by the dimensionless power coefficient, C_p , which is expressed as a ratio of the power the turbine extracts over the total power in the air.

Another major design factor is the speed at which the turbine is operating at relative to the air speed. This is again expressed as a dimensionless ratio that relates the tangential speed of the blade tip with the air velocity driving that blade called the tip-speed-ratio (TSR).

With these two factors, the blade's efficiency can be graphed over a range of speeds without explicitly determining the dimensions. Thus, if a model's dimensions are scaled accordingly to the specified ratios then the performance of the turbine can be accurately predicted by the power coefficient.

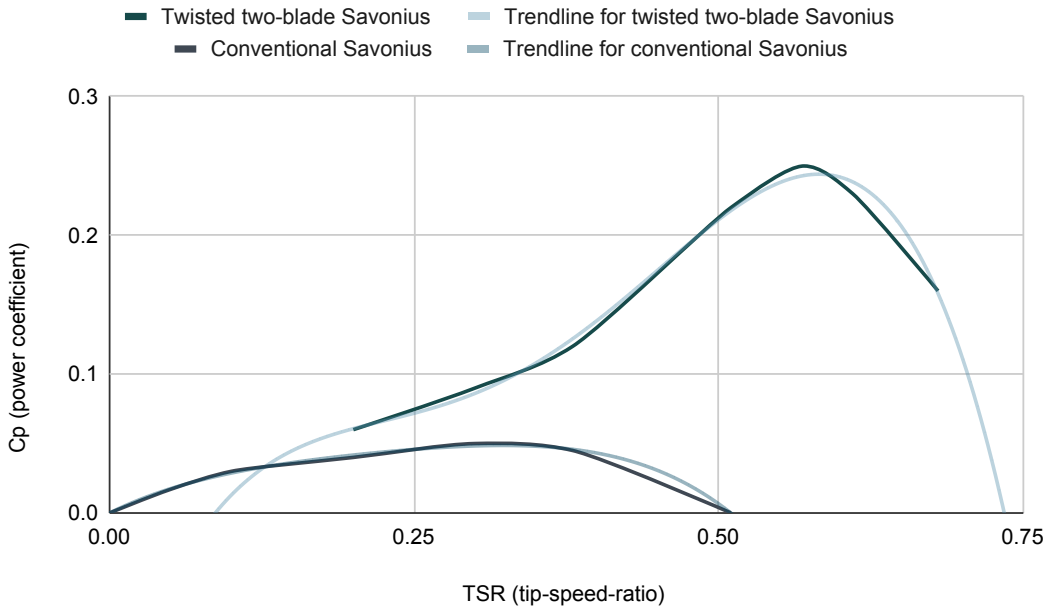


Figure 6: C_p vs TSR of the twisted two-blade Savonius design [19] and the conventional Savonius blade design [20].

The twisted two-bladed turbine design from [19] was chosen for its consistent performance over a large range of TSR. When compared to the conventional Savonius design it also has a much higher peak performance as can be seen in Figure 6. The design in [19] was computationally validated and the results were derived from computer fluid dynamics (CFD) simulations.

4.6 Turbine power output

To exploit the performance advantages of this turbine design, parameters were chosen to achieve the peak performance of the turbine design [19]. Thus, the TSR of 0.55 has been chosen which corresponds to a power coefficient of 0.25.

Due to the size constraints of the turbine fitting inside an air duct, the turbine is limited to have a diameter of 0.2 m and a height of 0.175 m. The design of the turbine can be seen in Figure 7.

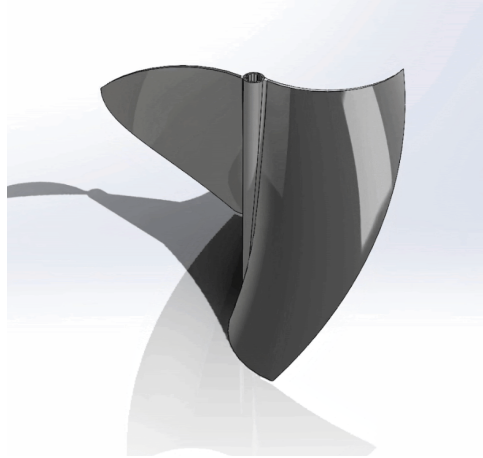


Figure 7: Twisted two-blade Savonius turbine.

The power output, rotational velocity and torque can be calculated from the minimum and maximum expected air velocities. The detailed calculations can be seen in Appendix H. The accelerated air velocities are:

$$v_{\min} = 10 \text{ m/s}$$
$$v_{\max} = 22 \text{ m/s}$$

Using the coefficient of power, C_p and Equation 4 for the power of fluid, the power output was found to be:

$$P_{\min} = 5.56 \text{ W}$$
$$P_{\max} = 57.07 \text{ W}$$

Then, using the TSR and the blade diameter, the rotational velocity of the turbine was determined to be:

$$\omega_{\min} = 55 \text{ rad/s (525 RPM)}$$
$$\omega_{\max} = 121 \text{ rad/s (1155 RPM)}$$

Lastly, the torque figures were calculated using P and ω to be:

$$Q_{\min} = 0.101 \text{ Nm}$$

$$Q_{\max} = 0.472 \text{ Nm}$$

These power figures and rotational velocities appear to be in accordance to the values achieved experimentally in [19] and also follow the expected increase in efficiency to the turbine designs tested in [20].

4.7 Drive train

Having determined the rotational speed of the turbine at the minimum air velocity and the required speed by the motor to be:

$$\omega_{\text{turbine}} = 525 \text{ RPM}$$

$$\omega_{\text{motor, required}} \approx 1100 \text{ RPM}$$

The aim of the drive train is to act as an interface between the turbine and the motor-generator, by matching the output of the turbine to the speed required by the generator. It is obvious that direct drive from the turbine to the motor-generator will not produce the required power output. Therefore, only drive trains that are able to increase or decrease the rotational speed were considered.

By the process of elimination, a belt drive system is deemed most appropriate for the product as it is low maintenance and produces a low amount of noise, addressing the customer need for a non-disruptive product (CN(5)) [21].

A chain drive system was deemed unsuitable as they are high maintenance, requiring frequent cleaning and tightening, and are less smooth, leading to unwanted noise pollution [21].

A geared drive system was eliminated because high tolerance requirements for the gears lead to higher manufacturing costs. According to [22] geared drive is also noisier in operation compared to belt drive violating a key customer need. Though gear drives are advantageous for high torque transmission, this was not necessary for this small scale turbine.

The technical analysis in Appendix I shows that the belt drive system in Figure 21 is of a valid design. It satisfies the required gearing ratio for the generator at the minimum turbine speed ω_{\min} and size constraints to fit within the turbine base.

5 Technical design and analysis: Fasteners

5.1 Designing for assembly

With the power requirements calculated, the technical design focus can shift to CAD and assembly. To align with the customer need of adaptability to infrastructure, design for assembly (DFA) is preferred as DFA precipices:

- Easy assembly and disassembly.
- Easy maintainability and replaceability of parts.
- Easy installation.

Therefore, the objectives of DFA is to:

- Minimise the number of parts and commercial off-the-shelf (COTS) components.
- Prefer simple assembly techniques especially with the maintenance of critical parts.

5.2 FEA optimisation process

A FEA optimisation process was developed to optimise the strength and mass distribution of the turbine parts. The process is shown as a flowchart in Figure 8 below.

To optimise a part, the load cases are first identified e.g. a shaft may experience torque, axial, and lateral forces. These load cases are then set up in Solidworks as static studies where the FEA was performed. The FEA provides stress and strain plots where the maximum stress and strain is obtained to calculate the modulus of elasticity:

$$\lambda = \frac{\sigma}{\epsilon} \quad (1)$$

Where:

- λ (Pa) is the modulus of elasticity.
- σ (Pa) is the stress.
- ϵ (dimensionless) is the strain.

The modulus of elasticity is then compared to the Young's modulus of the part's material. If the modulus of elasticity is greater than the Young's modulus then the part is optimised by adding or removing material to the part to redistribute the experienced stresses. This process is repeated until the modulus of elasticity is less than the Young's modulus.

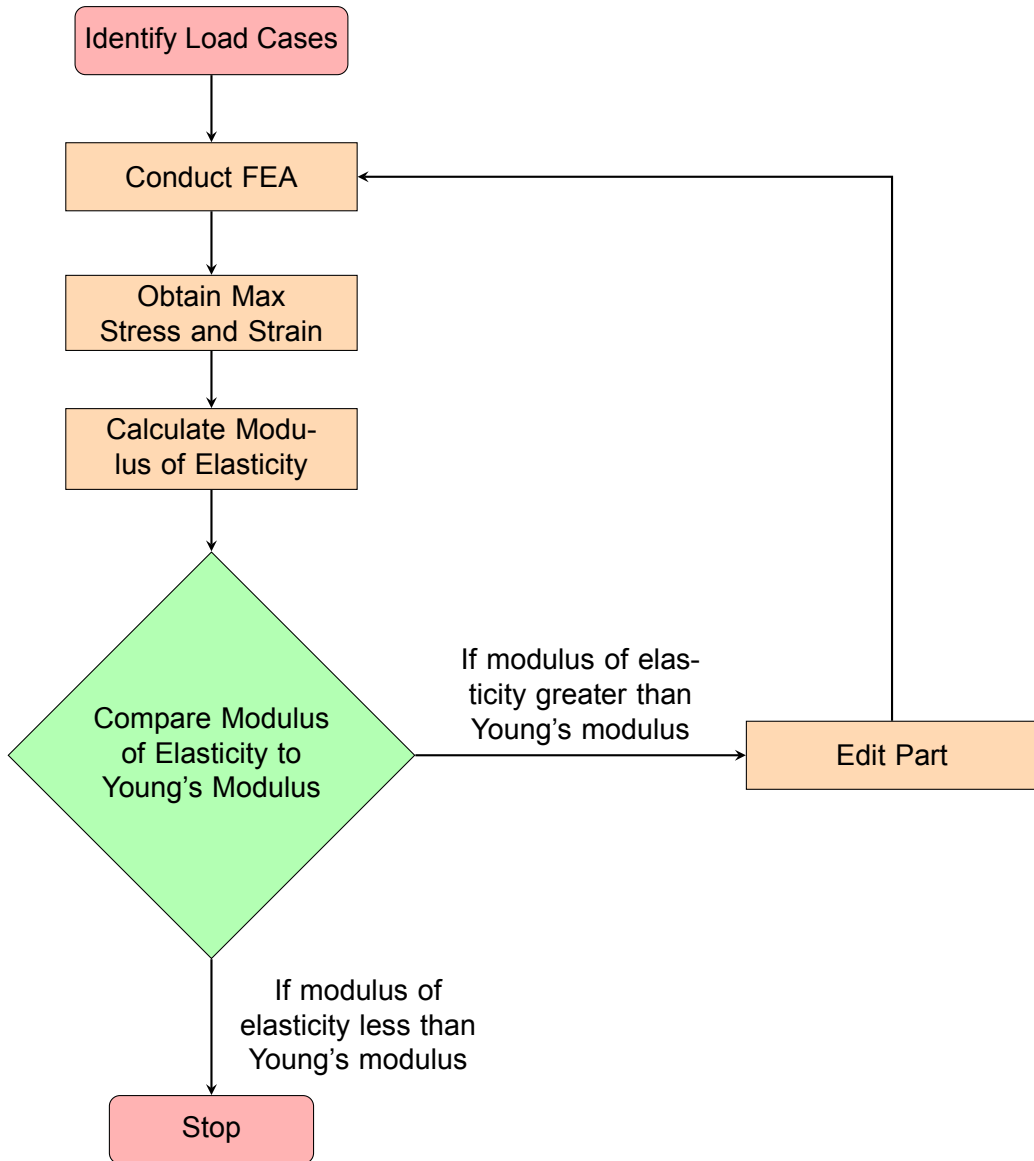


Figure 8: FEA optimisation process flowchart.

This process implicitly optimises the mass of the part which is a significant design factor for the rotor of the turbine. This is to decrease the required starting torque to overcome the inertia of the system.

5.3 Spline design

The design of the rotor requires the consideration of torque transfer from the turbine blades to the turbine shaft. There are various rotational fastening techniques that can be considered, therefore a trade-off study was performed using a weighted numerical evaluation matrix in Table 9.

Table 9: Weighted numerical evaluation matrix of rotational fastening techniques.

Fastener	Torque ($\times 2$)	Assembly ($\times 3$)	Reliability ($\times 1$)	Maintainability ($\times 3$)	Score
Single Solid	3	3	3	1	21
Spline	3	2	3	3	24
Feather Key	2	1	1	1	11
Sleeve Coupler	1	1	1	1	9

From Table 9, the spline feature (shown in Figure 9 with an initial width of 2 mm and height of 1 mm) is selected due to its highest score of 24. The turbine rotor can be split into a shaft and blade component which are meshed via the spline feature.

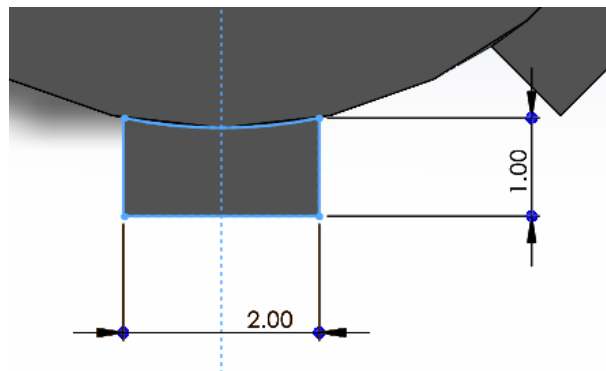


Figure 9: Spline diagram.

The spline of the shaft has two functions and thus has two significant loading cases (which are shown in Figure 10 below):

1. The spline acts as a shoulder to fix the axial movement of the rotor with respect to the stator component of the turbine.
2. The spline acts as a key to fix the rotational movement of the blades with the shaft.

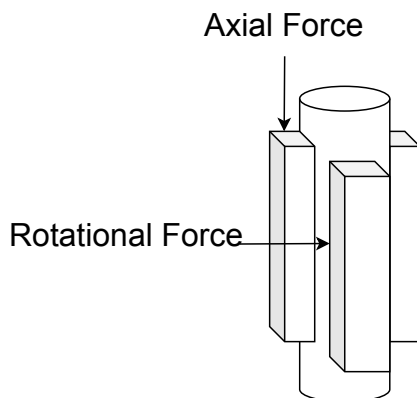


Figure 10: Spline loads.

For the axial load case, the axial load is simply the weight of the rotor components itself as the turbine blade is drag-based and thus produces no lift force:

$$F_{\text{axial, max}} = m_{\text{turbine + shaft}} \times g = 0.73 \text{ N}$$

The axial load after consideration of a FOS of 4.11 (justified in Appendix J) is:

$$F_{\text{axial, safe}} = 3 \text{ N}$$

The FEA optimisation process for the spline under axial load took two iterations with results tabulated in Table 10 (and documented in Appendix K). The iterative design process saw a chamfer added to the spline (which can be seen by comparing Figures 22 and 23).

Table 10: Iterative design of spline under axial load.

Iteration	Max Stress (10^5 Pa)	Max Strain (10^{-4})	Modulus of Elasticity (MPa)	Young's Modulus (MPa)	Design Change
1	2.602	1.407	1849	1400	-
2	2.263	1.735	1304	1400	Added 0.1 mm chamfer.

For the rotational load case, the load is the force of the fluid impacting the blade:

$$F_{\text{rotational, max}} = 2.59 \text{ N}$$

The rotational load after consideration of a FOS of 3.86 (justified in Appendix J) is:

$$F_{\text{rotational, safe}} = 10 \text{ N}$$

The FEA optimisation process for the spline under rotational load took two iterations with results tabulated in Table 11 (and documented in Appendix L). The iterative design process saw the shaft diameter increase from 8 mm to 10 mm (which can be seen by comparing Figures 24 and 25).

Table 11: Iterative design of spline under rotational load.

Iteration	Max Stress (10^5 Pa)	Max Strain (10^{-4})	Modulus of Elasticity (MPa)	Young's Modulus (MPa)	Design Change
1	12.78	8.694	1467	1400	-
2	7.149	5.218	1304	1400	Increase shaft diameter by 2 mm.

5.4 Circlip selection

Circlips are used to axially-fix components with respect to a shaft. For a shaft diameter of 10 mm, an external steel circlip with an internal diameter of 9.6 mm is selected - all circlips of this type conform to the requirements of the BS3673 [23].



Figure 11: Circlip failure cases.

Two possible failure cases for an axially-loaded circlip (shown in Figure 11) are evaluated with calculated FOS in Appendix M:

- An axial load is applied on the circlip causing a shear deformation (Figure 11a). This does not fail with a calculated FOS of 218.
- An axial load is applied on the circlip groove causing a yield deformation (Figure 11b). This does not fail with a calculated FOS of 5.12.

5.5 Turbine blade optimisation

The turbine blade after an initial design in Section 4.6 is further optimised using the FEA optimisation process which took two iterations with results tabulated in Table 12 (and documented in Appendix N). The iterative design process saw the blade base thickness increase from 2 mm to 3 mm (refer to Figure 28 for a sketch of the blade base).

Table 12: Iterative design of turbine blade.

Iteration	Max Stress (10^5 Pa)	Max Strain (10^{-4})	Modulus of Elasticity (MPa)	Young's Modulus (MPa)	Design Change
1	15.34	8.137	1885	1400	-
2	18.27	14.88	1228	1400	Increase blade thickness by 1 mm.

5.6 Bearing selection

Bearings are used to provide relative rotation between two components in an assembly. The turbine shaft is to be fixed by a bearing on both ends so that the rotor can spin freely. There are various bearing types that can be considered, therefore a trade-off study was performed using a weighted numerical evaluation matrix in Table 13.

Table 13: Weighted numerical evaluation matrix of bearing types.

Bearing Type	Axial Load ($\times 1$)	Radial Load ($\times 1$)	Cost ($\times 2$)	Score
Deep-Groove Ball	2	2	3	10
Thrust Ball	3	1	2	8
Cylindrical Roller	1	3	2	8
Angular Ball	3	3	1	8

From Table 13, the deep-groove ball bearing was selected due to its highest score of 10. To select a particular deep-groove ball bearing model, its physical constraints are considered:

- The inner diameter of the bearing is 10 mm to fasten the turbine shaft since the shaft diameter is 10 mm.
- The inner diameter of the outer race of the bearing must be greater than 20 mm (i.e. the outer diameter of the bearing should generally be greater than 22 mm) to give stator and rotor clearance since the diameter of the circlip is 18 mm.

From a gross market perspective of COTS bearings, Table 14 presents appropriate bearings with their specifications and rated loads:

Table 14: COTS bearings.

Bearing Model	Type	Inner diameter (mm)	Outer diameter (mm)	Static Load Rating (N)	Dynamic Load Rating (N)	Cost (AUD)
SS61900-2RS	Ball	10	22	1040	2160	8.75
R-2210X	Ball	10	22	1273	2679	9.645
61900	Ball	10	22	1270	2700	21.85
6000-2RS	Ball	10	26	1960	4620	6.13
6200-2RS	Ball	10	30	2360	5070	6.13

The identified load cases are the radial and axial load as shown in Figure 12.

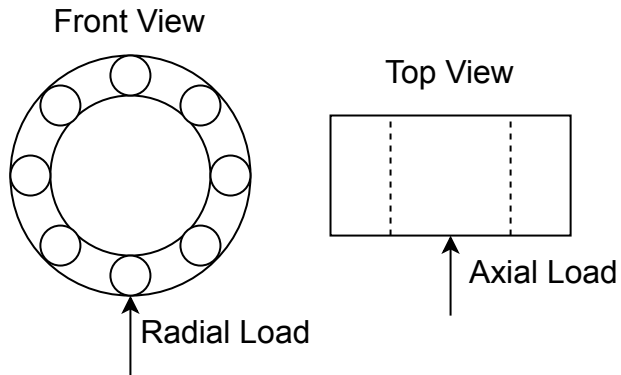


Figure 12: Bearing loads.

From Section 4.6, the max turbine torque is 0.472 Nm and max turbine rotational velocity is 1155 RPM. The radial and axial load is calculated (Appendix O) respectively as:

$$F_r = 24.84 \text{ N}$$

$$F_a = 0.73 \text{ N}$$

The equivalent dynamic bearing load was calculated as 24.84 N then compared to the dynamic load rating of the bearings from Table 14 which is tabulated in Table 15

Table 15: Comparison of dynamic load ratings and load.

Bearing Model	Equivalent Dynamic Bearing Load (N)	Dynamic Load Rating (N)	Satisfactory (yes/no)
SS61900-2RS	24.84	2160	yes
R-2210X	24.84	2679	yes
61900	24.84	2700	yes
6000-2RS	24.84	4620	yes
6200-2RS	24.84	5070	yes

Since any bearing with the given inner and outer diameter constraints is satisfactory under the provided load cases, the smallest and cheapest bearing model is selected i.e. SS61900-2RS.

5.7 Bolt selection

Bolts are used to locate and clamp the top and bottom lid to the case. This ensures that the lid can be shut firmly to reduce any vibrations caused by turbulence. It is important to use a detachable fastener in order keep the turbine accessible and easy to maintain.

The first load case for the fasteners on the top and bottom lid are similar. The suitability of the bolts were considered under the assumption that axial forces would only be experienced due to the weight of the system when it is not picked up by the bottom, for example, if it were to be picked up by the top lid. This is shown in Figure 13 below.

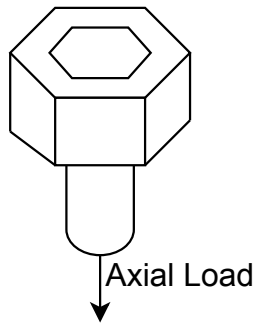


Figure 13: Bolt loads.

The force due to the weight of the system is equal to (Appendix P):

$$F = 49.05 \text{ N (downwards)}$$

To ensure that the bolt will fail before the threads start to strip, the thread shear area should be at least twice the tensile stress area. This gives us the appropriate length of

the bolt (Appendix P):

$$L = 8 \text{ mm}$$

M3 x 0.5 x 6 Grade 4.8 bolts with M3 x 0.5 x 9.8 threaded inserts are suitable (as justified in Appendix P), since they are cheap and easily replaceable. Threaded inserts withstand vibration without loosening, and do not stick out the way nuts do. This allows for the screen to fit into the case with minimal interference.

Under these conditions, the FOS is equal to 341 (as calculated in Appendix P) which is greater than the recommended value detailed in Appendix J.

The second load case regards minimising damage to the surrounding material and maximising the strength of the fastener. Bolts should be spaced 1.5 x bolt diameter between each other and from the edge. Therefore, the top and bottom lids will both be secured with four bolts each, spaced apart as shown in the top view of the top lid in Section 6.

External shear forces may be present due to vibration but they were considered to be negligible.

5.8 Vent interface

The turbine interface with the vent must be considered and should be adaptable to a range of air duct sizes without a loss of integrity to the air duct structure. There exists various interfacing techniques, therefore a trade-off study was performed using a weighted numerical evaluation matrix in Table 16.

Table 16: Weighted numerical evaluation matrix of vent interfaces.

Interface Type	Installation Effort ($\times 3$)	Cost ($\times 1$)	Design Complexity ($\times 2$)	Various Vent Sizes ($\times 3$)	Score
Bolting	1	2	2	1	12
Anti-Slip Pad	3	3	3	3	27
Plunger Lock	2	1	1	2	15

From Table 16, the anti-slip pad was selected due to its highest score of 27. A slipping calculation (Appendix Q) was performed to determine the feasibility of rubber pads on an aluminium vent surface. The frictional force was calculated to be greater than the pushing force of the fluid, therefore the assembly will not slip:

$$F_{\text{fluid, safe}} = 10 \text{ N} < 39.24 \text{ N} = F_{\text{friction}}$$

A tipping calculation (Appendix R) was also performed since the turbine was not secured. The moment weight was calculated to be greater than the tipping moment of the fluid, therefore the assembly will not tip:

$$\tau_{\text{fluid, safe}} = 1.25 \text{ Nm} < 6.62 \text{ Nm} = \tau_{\text{weight}}$$

6 CAD model

The CAD model of the final design concept is shown in Figure 14 below. A three-quarter view of the model can be seen in Figure 31 of Appendix S.

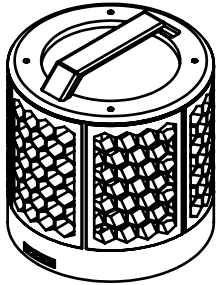
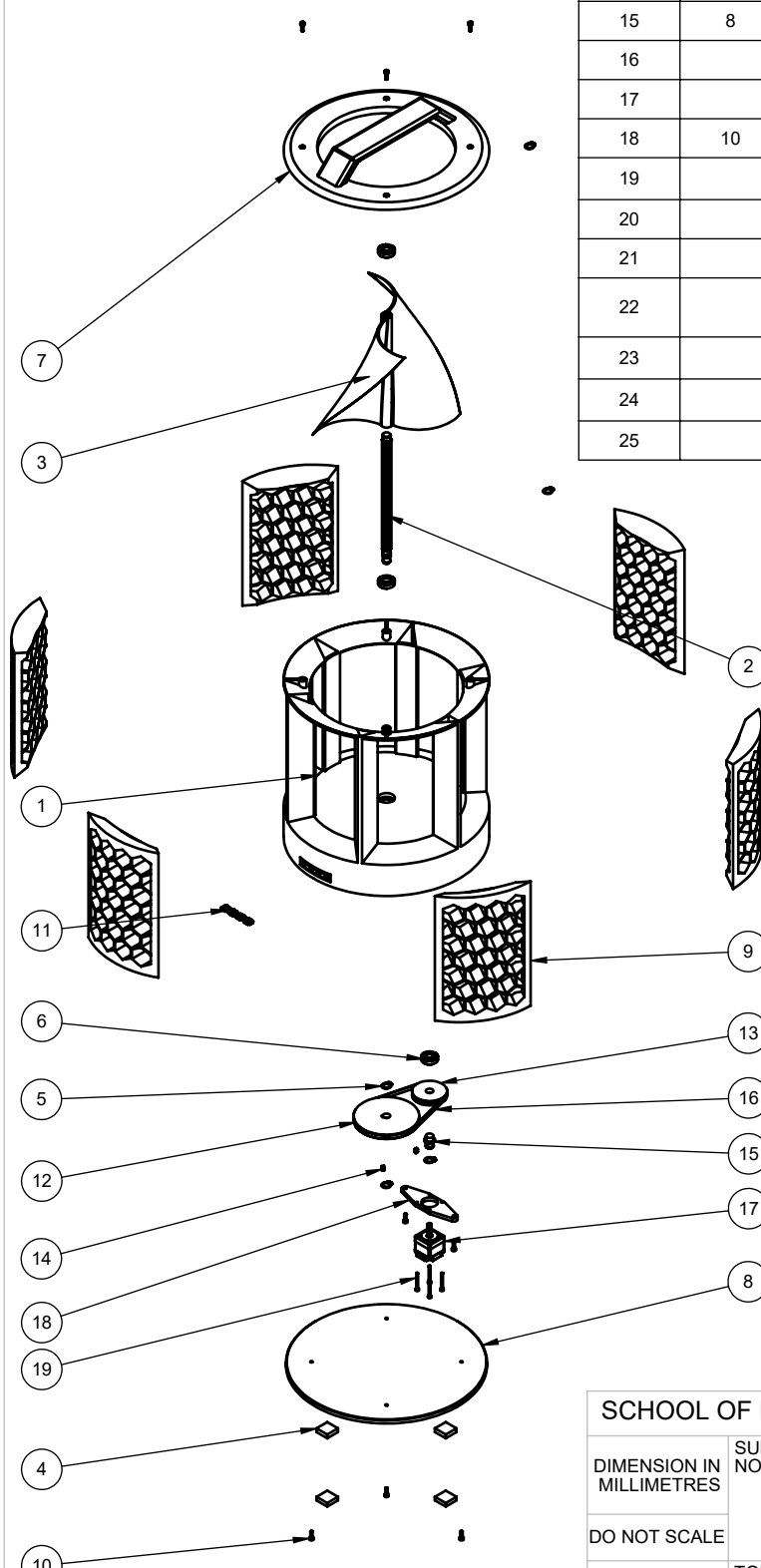


Figure 14: CAD model of InVent turbine.

The following pages include an assembly drawing of the turbine with a Bill of Materials (BOM) and 2D engineering drawings of the various components that were designed for the InVent turbine. A more detailed BOM is available in Appendix T.

A prototype of the turbine in Appendix U was used to demonstrate and validate the concept.

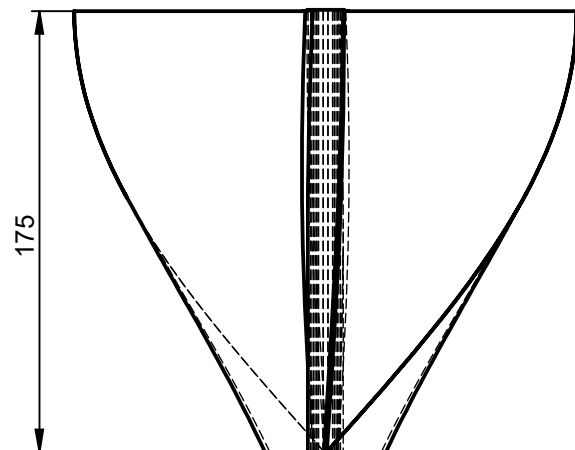
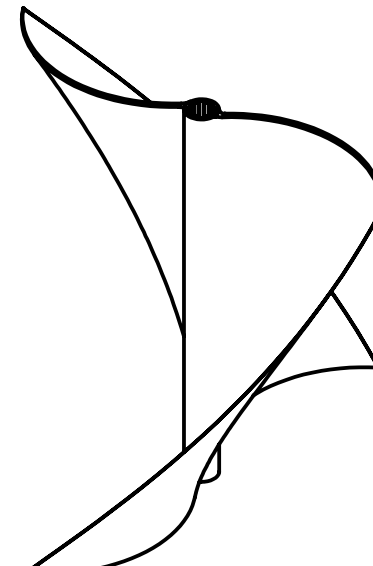
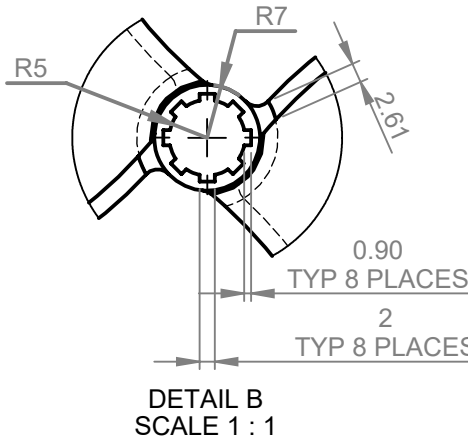
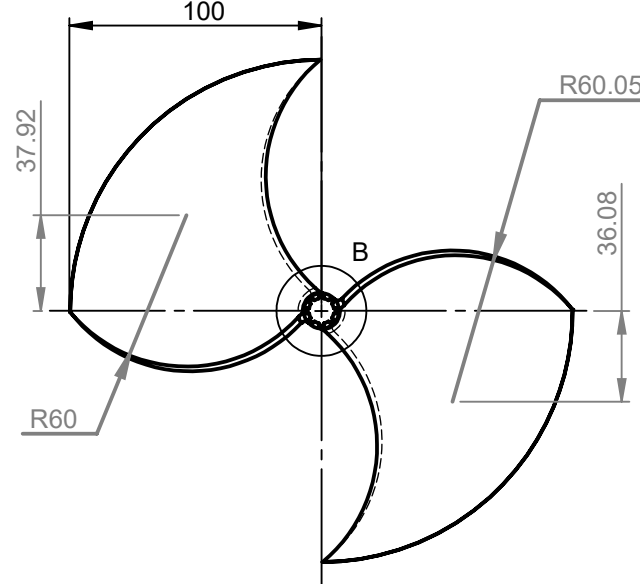
PART NO.	DRAW NO.	NAME	DESC.	MTL	QTY
1	3	CASE		ABS PLASTIC	1
2	7	SHAFT		ABS PLASTIC	1
3	1	BLADE		ABS PLASTIC	1
4		FOOT		RUBBER	4
5		CIRCLIP	EXTERNAL 10 MM BS3673	STEEL	5
6		BEARING	SS61900-2RS	STEEL	3
7	9	TOP LID		ABS PLASTIC	1
8	2	BOTTOM LID		ABS PLASTIC	1
9	6	SCREEN		RUBBER	6
10		M3 HEX SOCKET BOLT	AS 1420 - M3 X 10-N	STEEL	10
11		USB C			4
12	5	DRIVING PULLEY		ABS PLASTIC	1
13	4	DRIVEN PULLEY		ABS PLASTIC	1
14		FEATHER KEY	7 X 3 X 3	STEEL	2
15	8	SHORT SHAFT		ABS PLASTIC	1
16		BELT		RUBBER	1
17		NEMA11			1
18	10	NEMA11 MOUNT			1
19		M2.5 HEX SOCKET BOLT	AS 1420 - M2.5 X 25-N	STEEL	4
20		LIPO BATTERY	7 V, 1 AHR		1
21		BRIDGE RECTIFIER	2 A, 50 V, 4-PIN		1
22		ELECTROLYTIC CAPACITOR	4700 UF, 25 V		1
23		VOLTAGE REGULATOR	2 A, 12 V, 3-PIN		1
24		ARDUINO WIFI SHIELD			1
25		ARDUINO UNO			1



ISOMETRIC VIEW

SCHOOL OF MECHANICAL AND MANUFACTURING ENGINEERING - UNSW					
DIMENSION IN MILLIMETRES	SURFACE FINISH UNLESS NOTED OTHERWISE		DRAWN BY		TITLE TURBINE DRAWING NUMBER 11
	NIKKI FANG (Z5310518)		CHECKED BY		
DO NOT SCALE	DAN NGUYEN (Z5206032)		APPROVED BY		FIRST RELEASE DATE 25/11/2022
	DAN NGUYEN (Z5206032)		REV		
TOLERANCE UNLESS NOTED OTHERWISE	±0.05		SCALE	DATE	A3
	QTY	MATL	1:7	1	

EXPLODED ISOMETRIC VIEW



ALL FILLETS ARE R4 UNLESS STATED OTHERWISE

AS1100

SCHOOL OF MECHANICAL AND MANUFACTURING ENGINEERING - UNSW

SURFACE FINISH UNLESS
NOTED OTHERWISE

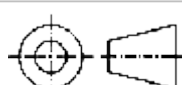
✓

TITLE

BLADE

DRAWN BY
CATHERINE CHENG (Z5310517)

DATE
23/11/2022



TOLERANCE
 ± 0.05

DRAW NO.
1

MATL
ABS PLASTIC

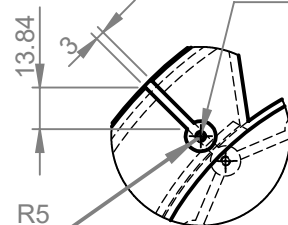
SCALE
1:3

DO NOT
SCALE

DIMENSION IN
MILLIMETRES

A4

4 x ϕ 2.50 \downarrow 11.50
 \checkmark M3 - 6H \downarrow 10



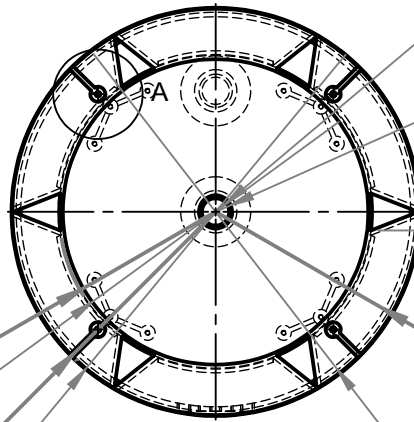
DETAIL A
SCALE 2 : 5

R103.42

ϕ 202

R134.36

ϕ 269.877



TOP VIEW

ϕ 18 THRU

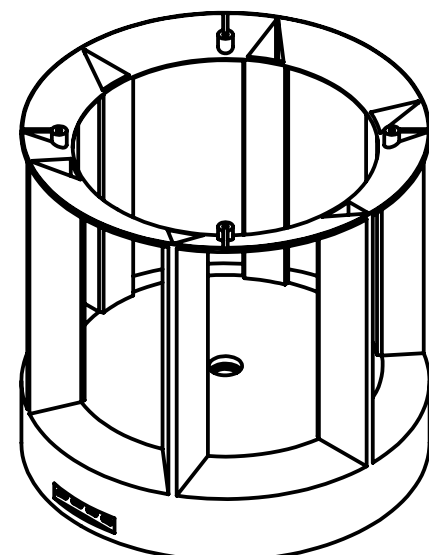
ϕ 18 THRU

ϕ 22 \downarrow 6

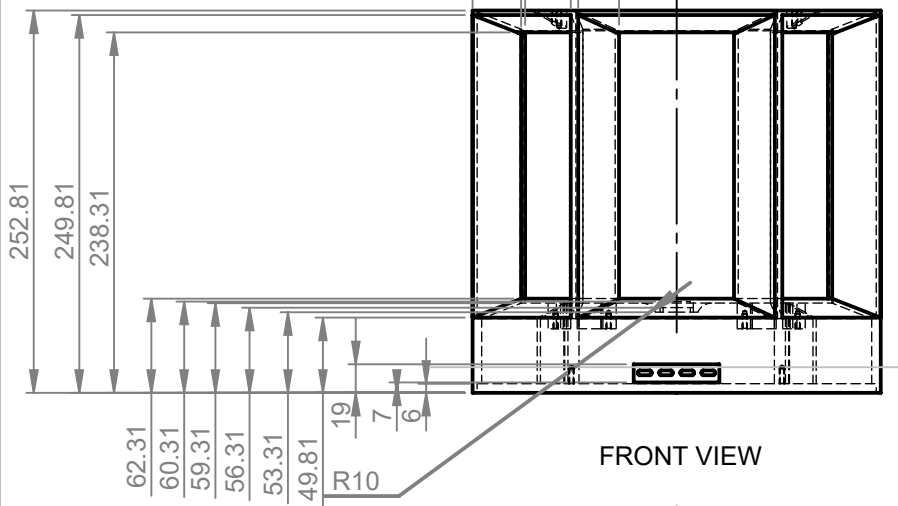
0.78
12.31

R128.94

ϕ 263.877



ISOMETRIC VIEW



FRONT VIEW

ϕ 46.330

ϕ 28

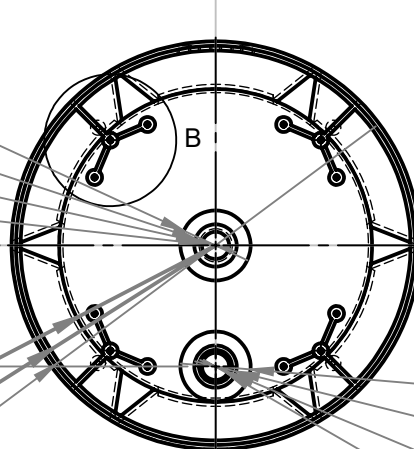
ϕ 22

ϕ 18

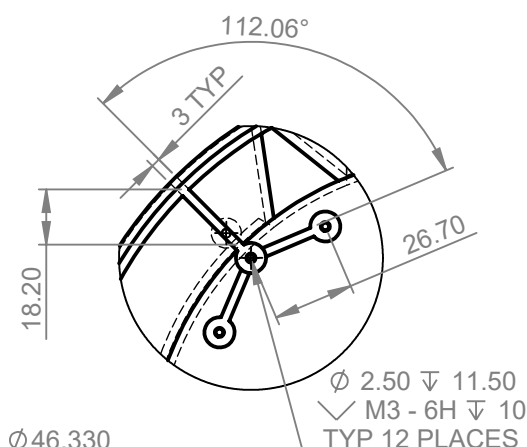
R103.42

R128.94

ϕ 263.877



BOTTOM VIEW



DETAIL B
SCALE 2 : 5

SCHOOL OF MECHANICAL AND MANUFACTURING ENGINEERING - UNSW

SURFACE FINISH UNLESS
NOTED OTHERWISE



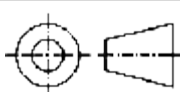
TITLE

CASE

DRAWN BY
NIKKI FANG (Z5310518)

DATE

25/11/2022

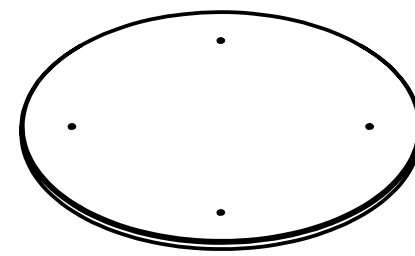
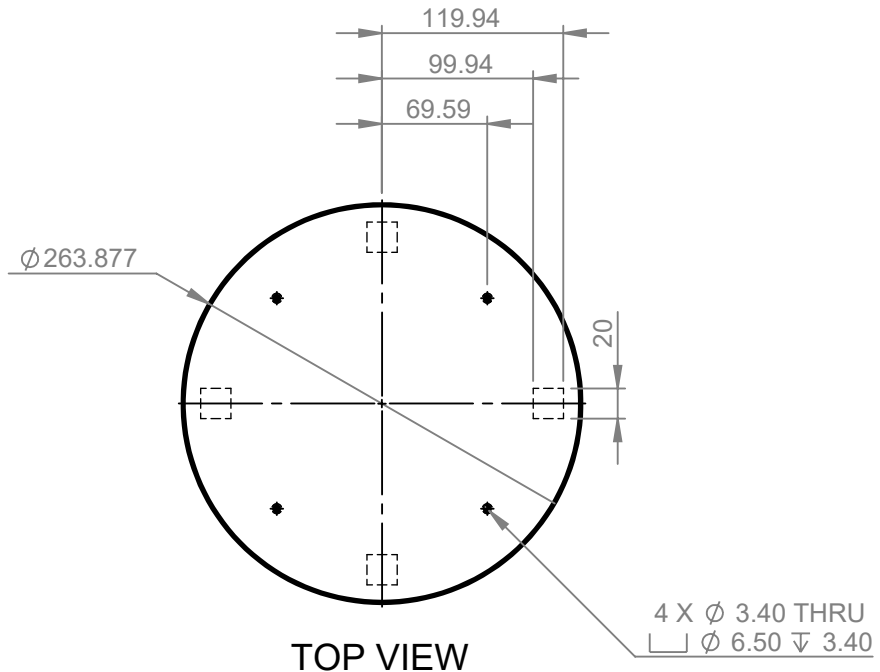


TOLERANCE

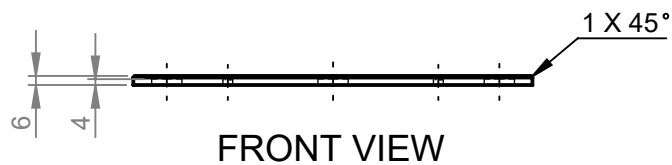
\pm 0.05

DRAW NO.

3

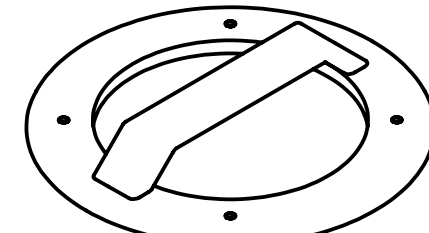
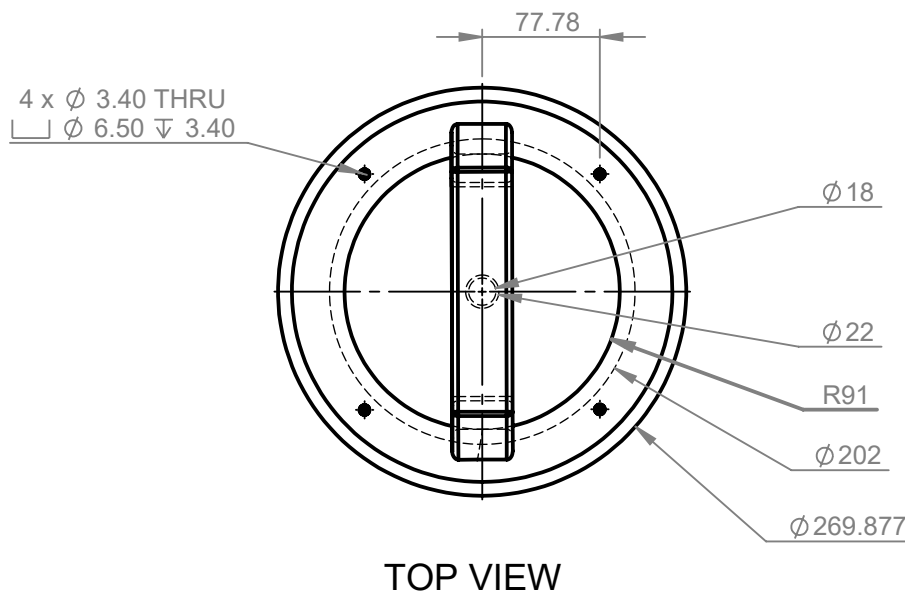


ISOMETRIC VIEW

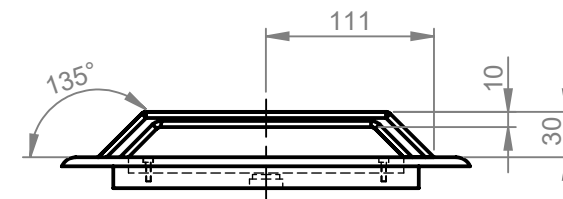
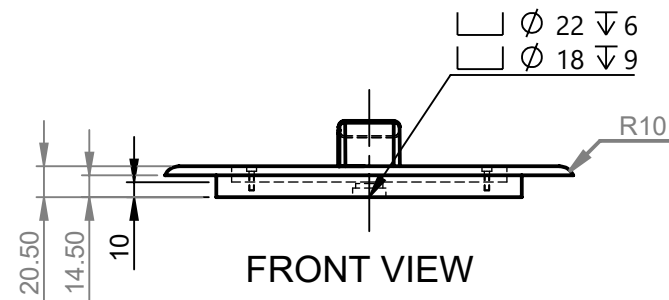


AS1100

SCHOOL OF MECHANICAL AND MANUFACTURING ENGINEERING - UNSW			
SURFACE FINISH UNLESS NOTED OTHERWISE		TITLE DRAWN BY CATHERINE CHENG (Z5310517)	BOTTOM LID DATE 23/11/2022
	TOLERANCE ± 0.05		
	MATL ABS PLASTIC	SCALE 1:5	DO NOT SCALE
A4			



ISOMETRIC VIEW

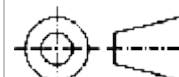


ALL FILLETS ARE R4 UNLESS STATED OTHERWISE

AS1100

SCHOOL OF MECHANICAL AND MANUFACTURING ENGINEERING - UNSW

SURFACE FINISH UNLESS
NOTED OTHERWISE



TOLERANCE
 ± 0.05

✓
DRAW NO.
9

TITLE
TOP LID

DRAWN BY
CATHERINE CHENG (Z5310517)

DATE
23/11/2022

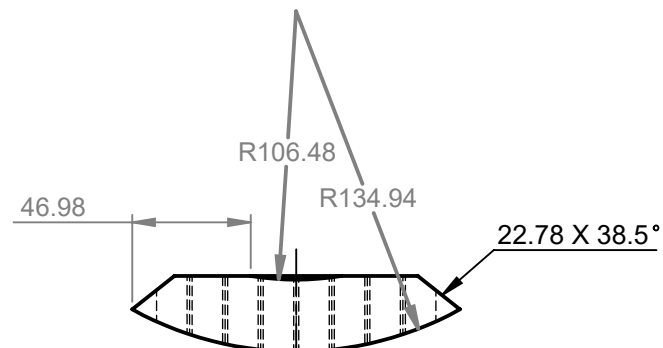
MATL
ABS PLASTIC

SCALE
1:2

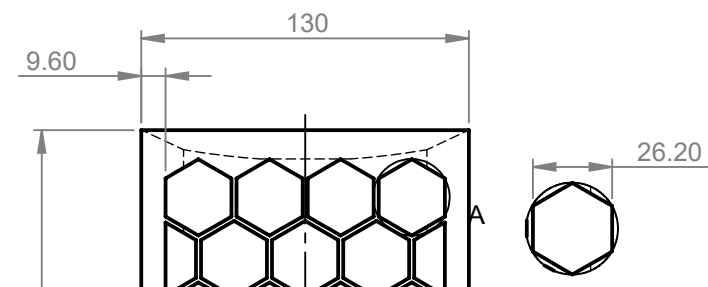
DO NOT
SCALE

DIMENSION IN
MILLIMETRES

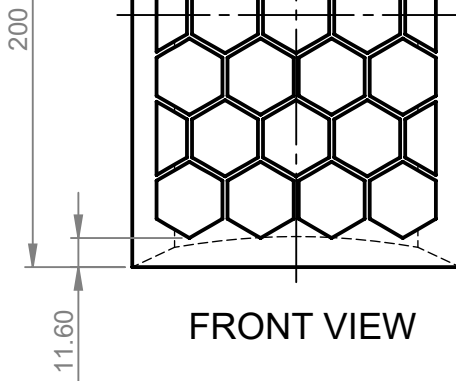
A4



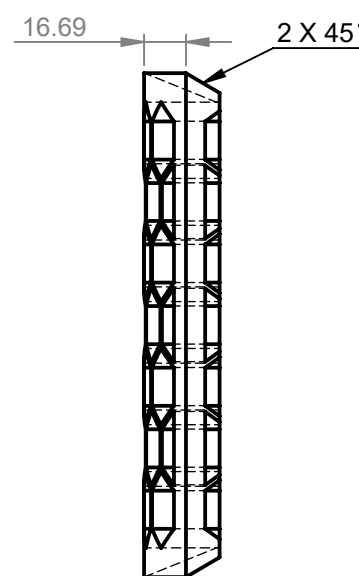
TOP VIEW



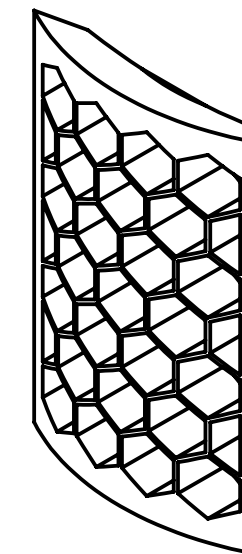
DETAIL A
SCALE 2 : 5



FRONT VIEW



LEFT VIEW



ISOMETRIC VIEW

AS1100

SCHOOL OF MECHANICAL AND MANUFACTURING ENGINEERING - UNSW

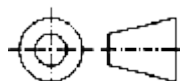
SURFACE FINISH UNLESS
NOTED OTHERWISE



TITLE SCREEN

DRAWN BY
NIKKI FANG (Z5310518)

DATE
24/11/2022



TOLERANCE
 ± 0.05

DRAW NO.
6

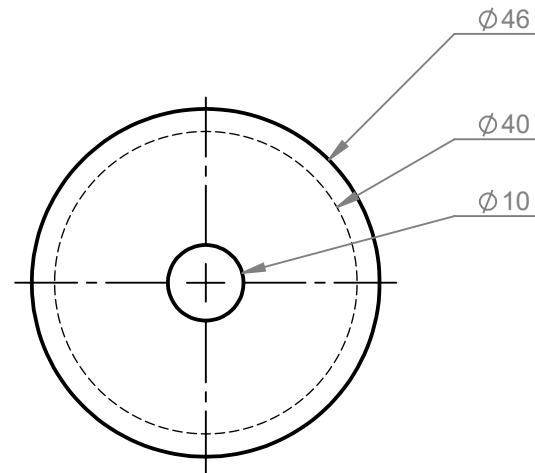
MATL
RUBBER

SCALE
1:5

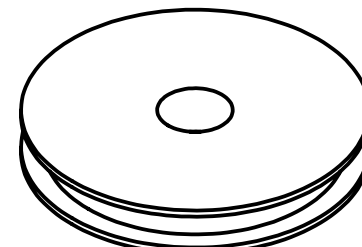
DO NOT
SCALE

DIMENSION IN
MILLIMETRES

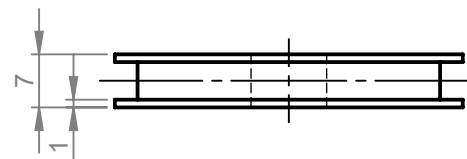
A4



TOP VIEW



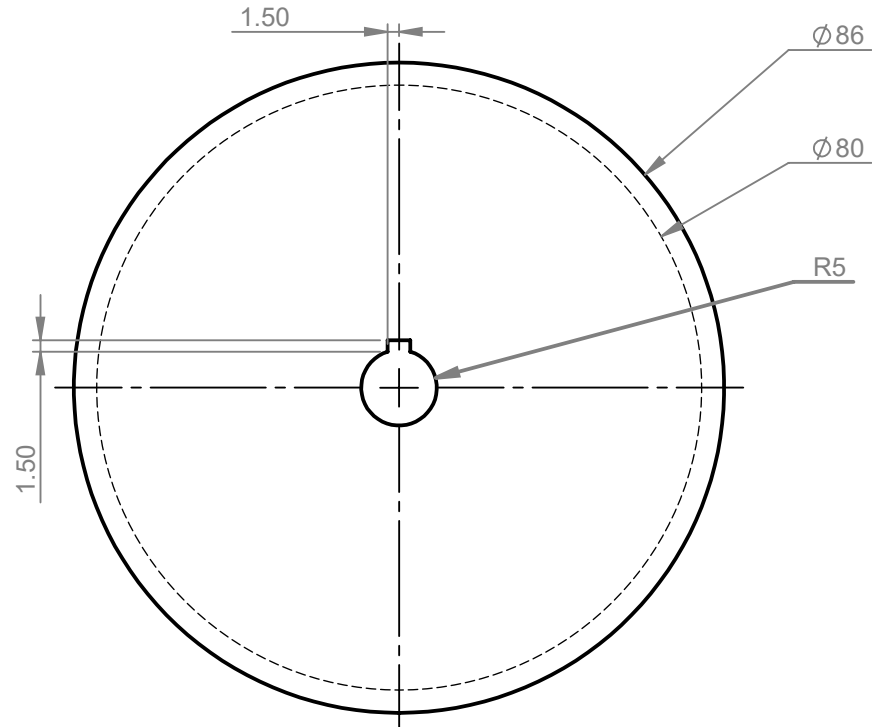
ISOMETRIC VIEW



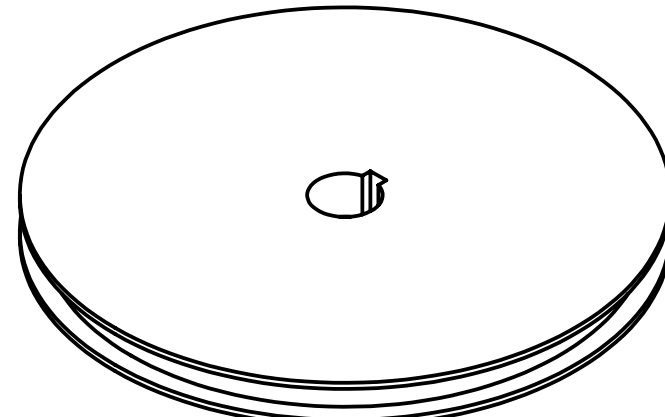
FRONT VIEW

AS1100

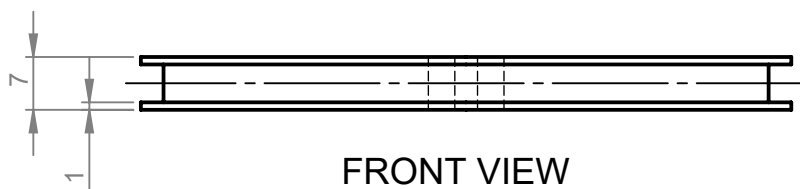
SCHOOL OF MECHANICAL AND MANUFACTURING ENGINEERING - UNSW					
SURFACE FINISH UNLESS NOTED OTHERWISE			TITLE DRAWN BY NIKKI FANG (Z5310518)		
	TOLERANCE ± 0.05	DRAW NO. 4	DRIVEN PULLEY		DATE 24/11/2022
		MATL ABS PLASTIC	SCALE 1:1	DO NOT SCALE	DIMENSION IN MILLIMETRES A4



TOP VIEW

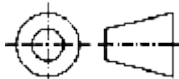


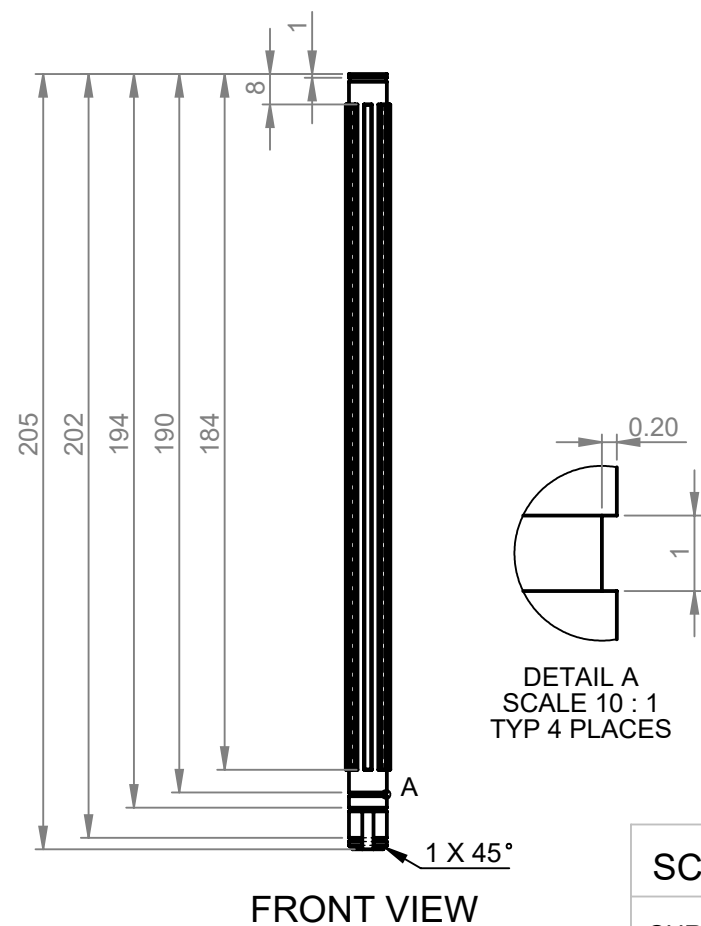
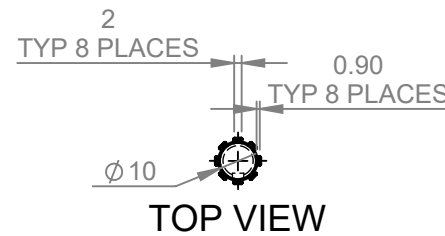
ISOMETRIC VIEW



FRONT VIEW

AS1100

SCHOOL OF MECHANICAL AND MANUFACTURING ENGINEERING - UNSW			
SURFACE FINISH UNLESS NOTED OTHERWISE		<input checked="" type="checkbox"/>	TITLE DRIVING PULLEY
	TOLERANCE ± 0.05	DRAW NO. 5	DRAWN BY NIKKI FANG (Z5310518)
			DATE 24/11/2022
MATL ABS PLASTIC	SCALE 1:1	DO NOT SCALE	DIMENSION IN MILLIMETRES
A4			



ISOMETRIC VIEW

AS1100

SCHOOL OF MECHANICAL AND MANUFACTURING ENGINEERING - UNSW

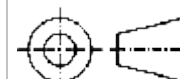
SURFACE FINISH UNLESS
NOTED OTHERWISE



TITLE SHAFT

DRAWN BY
CATHERINE CHENG (Z5310517)

DATE
23/11/2022



TOLERANCE
 ± 0.05

PART NO.
7

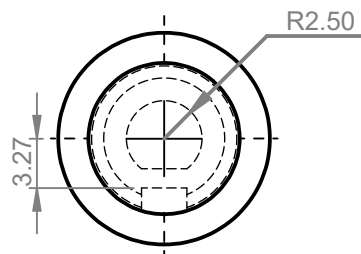
MATL
ABS PLASTIC

SCALE
1:2

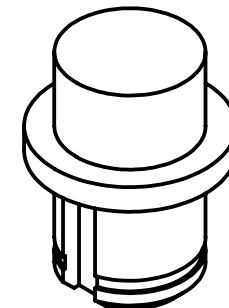
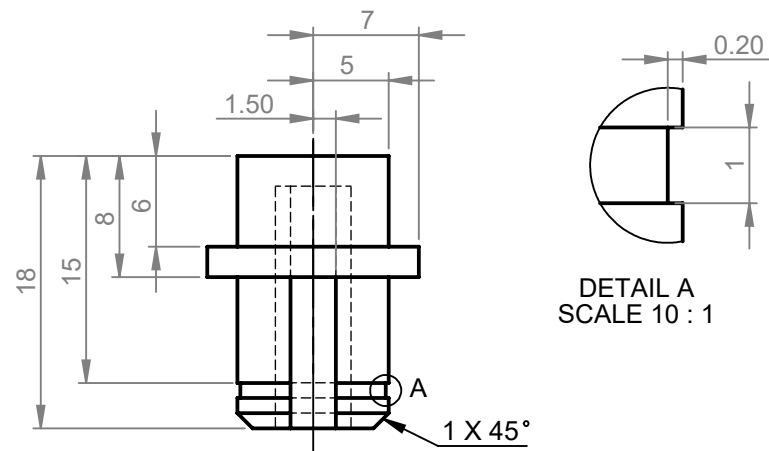
DO NOT
SCALE

DIMENSION IN
MILLIMETRES

A4



TOP VIEW



ISOMETRIC VIEW

AS1100

SCHOOL OF MECHANICAL AND MANUFACTURING ENGINEERING - UNSW			
SURFACE FINISH UNLESS NOTED OTHERWISE		TITLE SHORT SHAFT	
	TOLERANCE	DRAWN BY CATHERINE CHENG (Z5310517)	
		DATE 23/11/2022	
	DRAW NO. 8	MATL ABS PLASTIC	SCALE 2:1
		DO NOT SCALE	DIMENSION IN MILLIMETRES A4

7 Conclusion

The InVent system is a potentially life-saving engineering solution for the ever-increasing concern about air quality in workplaces in urban areas. While other airborne hazard sensing systems exist, the InVent system is innovative and novel. Powered by exhausted air, it is a fully self-sufficient system that delivers reliable performance. Designed with users in mind, the product is lightweight, modular, affordable, intuitive to install and easy to maintain.

Through a thorough investigation of user stories, customer needs and functional requirements, this suitable design was refined. Rigorous technical analysis techniques such as calculations, as found in this report, were used to validate that the solution is feasible, effective and safe. There were many concepts and iterations of the solution as calculations uncovered contradictions or requirements that were not being met. Within the team, it was challenging as full-time university students to balance other commitments and stay meticulous with this project. Ultimately, through health and through sickness, this was overcome with constant communication and effective collaboration.

With the product's technical specifications selected and justified, the system is ready for further development. Future possible work includes creating a full working prototype to validate the design by gathering data about the power generation of the turbine and surveying users about their experience using the system. The InVent system has the potential to save hundreds of thousands of lives and improve the working standards of millions more by monitoring air quality and keeping the workplace safe.

References

- [1] H. Ritchie and M. Roser, "Urbanization." <https://ourworldindata.org/urbanization#citation>, September 2018. Accessed: 23-11-2022.
- [2] United Nations, "Un health agency warns of rise in urban air pollution." <https://www.un.org/sustainabledevelopment/blog/2016/05/un-health-agency-warns-of-rise-in-urban-air-pollution-with-poorest-cities-most-at-risk/>, May 2016. Accessed: 23-11-2022.
- [3] World Health Organization, "WHO/ILO: Almost 2 million people die from work-related causes each year." <https://www.who.int/news/item/16-09-2021-who-ilo-almost-2-million-people-die-from-work-related-causes-each-year>, September 2021. Accessed: 23-11-2022.
- [4] W. D. Labaki and M. K. Han, "Chronic respiratory diseases: a global view," *The Lancet*, vol. 8, no. 6, pp. 531–533, 2020.
- [5] A. R. Winslow, "Urban wind generation: Comparing horizontal and vertical axis wind turbines at clark university in worcester, massachusetts," 2017.
- [6] J. Scheiman, "Considerations for the installation of honeycomb and screens to reduce wind-tunnel turbulence," 08 1981.
- [7] K. A. Adeyeye, N. Ijumba, and J. Colton, "The effect of the number of blades on the efficiency of a wind turbine," *IOP Conference Series: Earth and Environmental Science*, vol. 801, p. 012020, June 2021.
- [8] L. Hartman, "Wind turbines: the bigger, the better." <https://www.energy.gov/eere/articles/wind-turbines-bigger-better#:~:text=A%20turbine%20with%20longer%20blades,available%20for%20wind%20development%20nationwide>.
- [9] T. V. Nguyen, T. K. Tran, H. H. Dinh, and N. H. B. Ho, "Bladeless wind turbines," in *Science-Policy Brief for the Multistakeholder Forum on Science, Technology and Innovation for the SDGs*, 2022.
- [10] D. J. Y. Villarreal, "Viv resonant wind generators," 06 2018.
- [11] A. Soomro, "Vortex bladeless wind turbines,"
- [12] Wikipedia, "Betz's law." https://en.wikipedia.org/wiki/Betz%27s_law, October 2022.
- [13] U. Kafader, "DC motors as generators." <https://drive.tech/en/stream-content/dc-motors-as-generators>. Accessed: 23-11-2022.

- [14] REUK.co.uk, “Electricity with stepper motors.” <http://www.reuk.co.uk/wordpress/wind/electricity-with-stepper-motors/>. Accessed: 23-11-2022.
- [15] D. Davis, “MKII 5 watt 3d printable wind turbine.” <https://www.thingiverse.com/thing:2060281>. Accessed: 23-11-2022.
- [16] D. Bernoulli, *Hydrodynamica, sive de viribus et motibus fluidorum commentarii: opus academicum ab auctore, dum Petropoli ageret, congestum*. ETH-Bibliothek Zürich, Rar 5503, 1738.
- [17] A. Kragten, “The Darrieus rotor, a vertical axis wind turbine (VAWT) with only a few advantages and many disadvantages,” Tech. Rep. KD 215, Engineering office Kragten Design, Populierenlaan 51, 5492 SG Sint-Oedenrode, the Netherlands, December 2004.
- [18] ScienceDirect, “Savonius wind turbine.” <https://www.sciencedirect.com/topics/engineering/savonius-wind-turbine>, 2022. Accessed: 23-11-2022.
- [19] T. A. Mazari, T. Hussain, and M. S. Jamali, “Design and analysis of vertical axis wind turbine on small scale energy production,” *International Journal of Scientific & Engineering Research*, vol. 10, no. 4, 2019.
- [20] C. Sranpat, S. Unsakul, P. Choljararux, and T. Leephakpreeda, “CFD-based performance analysis on design factors of vertical axis wind turbines at low wind speeds,” in *International Conference on Alternative Energy in Developing Countries and Emerging Economies*, (Bangkok, Thailand), 2017.
- [21] TVS Motor, “Chain vs belt vs shaft drive: Motorcycle final drive systems explained with their characteristics.” <https://www.tvsmotor.com/Media/Blog/chain-vs-belt-vs-shaft-drive-motorcycle-final-drive-systems-explained-with-their-characteristics/>. Accessed: 23-11-2022.
- [22] L. Burgess, “Which is better: Gear drive or belt and pulley drive system?” <https://www.design-engineering.com/which-is-better-gear-drive-or-belt-and-pulley-drive-system-1004038188/>. Accessed: 23-11-2022.
- [23] British Standards Institution, “Specification for spring retaining rings - carbon steel circlips - metric series.” https://infostore.saiglobal.com/en-au/standards/bs-3673-4-1977-1977-231470_saig_bsi_bsi_542133/.
- [24] Engineering ToolBox, “Air duct velocities.” https://www.engineeringtoolbox.com/flow-velocity-air-ducts-d_388.html, 2003.
- [25] Engineering ToolBox, “Rectangular ducts - dimensions.” https://www.engineeringtoolbox.com/rectangular-ducts-d_1010.html, 2005.

- [26] D. Nguyen, “Battery.” <https://gitlab.com/dennuguyen/robotics-handbook/-/tree/master/battery>, 2022.
- [27] Stepper Online, “Nema 11 - 28 x 28mm.” <https://www.omc-stepperonline.com/nema-11-stepper-motor>. Accessed: 23-11-2022.
- [28] Nanotec, “Internal rotor motors.” <https://en.nanotec.com/products/2265-brushless-dc-motors-rpm-w-watt>. Accessed: 23-11-2022.
- [29] Flettner Ventilator, “Flettner TXC-2™ Ventilator.” <https://www.flettner.co.uk/products/flettner-tcx-2/>. Accessed: 23-11-2022.
- [30] A. Kovacevic, “Mechanical analysis: Belt and chain drives.” <http://www.staff.city.ac.uk/~ra600/ME2105/Analysis/ME2104-A-3.pdf>. Accessed: 23-11-2022.
- [31] W. Musial and C. Butterfield, “Using partial safety factors in wind turbine design and testing.” <https://www.nrel.gov/docs/legosti/old/23257.pdf>, June 1997.
- [32] Engineering Toolbox, “Factors of safety.” https://www.engineeringtoolbox.com/factors-safety-fos-d_1624.html, 2010.
- [33] MatWeb, “Overview of materials for acrylonitrile butadiene styrene (abs), extruded.” <https://www.matweb.com/search/DataSheet.aspx>. Accessed: 24-11-2022.
- [34] Smalley, “Ring design load capacity.” <https://www.smalley.com/ring-design/load-capacity>. Accessed: 24-11-2022.
- [35] Engineering Toolbox, “Young’s modulus, tensile strength and yield strength values for some materials.” https://www.engineeringtoolbox.com/young-modulus-d_417.html. Accessed: 24-11-2022.
- [36] RS PRO, “Rs pro deep groove ball bearing - plain race type, 10mm i.d, 19mm o.d.” <https://au.rs-online.com/web/p/ball-bearings/6189979>.
- [37] A. T. C. for MSC.ADAMS, “Material contact properties table.” atc.sjf.stuba.sk/files/mechanika_vms_ADAMS/Contact_Table.pdf.

Biography

Catherine Cheng



Catherine is a 3rd year aerospace engineering and computer science student. There are few things in life that bring her more joy than the engineering design process. These include: the pleasant walking distance from Ainsworth to AGSM, making tables in \LaTeX , and aptly-timed fire alarms.

Courtney Coates



Court is a 5th year mechatronic engineering student, who forgot to take this class earlier in her degree. When not writing executive summaries, she can be found either in Willis Annexe 204 trying to make a thesis, or at home pretending her thesis does not exist.

Dan Nguyen



5th year.

James Jiang



James is a 5th year mechatronics engineering and computer science student who was hoping to take the TAFE based equivalent of this course after the pandemic. Luckily, he did not have to use a single tool throughout the term which is why he probably still has all his fingers. After long days of report writing, he finds nothing more rewarding than seeing the \LaTeX file compile in Arial.

Melissa Thein



Melissa is a 2nd year mechatronics engineering student. After a long day of conducting user surveys, she appreciates nothing more than Uncle Tetsu's cheesecakes and ergonomic swivel chairs.

Nikki Fang



Nikki is a 3rd year mechatronics engineering and computer science student. After completing this course, she cannot wait to write more in \LaTeX , use more SOLIDWORKS and coming up with witty names for energy harvesting devices.

Appendix A. Technical analysis of wind energy within air vents

To calculate the energy of a moving object one must consider the equation for kinetic energy:

$$E_{\text{kinetic}} = \frac{1}{2}mv^2 \quad (2)$$

Where:

- E_{kinetic} (J) is kinetic energy.
- m (kg) is the object mass.
- v (m/s) is the velocity.

However, air particles have a very low mass so the mass flow in a specific area must be considered instead of the mass of an air particle. This gives:

$$\frac{dm}{dt} = \rho Av \quad (3)$$

Where:

- ρ (kg/m^3) is the fluid density.
- A (m^2) is the cross-sectional surface area that the fluid flows through.
- v (m/s) is the fluid velocity.

Substituting Equation 3 into Equation 2 gives the power of fluid equation:

$$P_{\text{fluid}} = \frac{1}{2}\rho Av^3 \quad (4)$$

Where P_{fluid} is the power of the fluid in watts. Thus, air can be treated as a fluid with a density of $\rho = 1.225 \text{ kg/m}^3$. The cross-sectional surface area A can be the size of the air duct to determine the power of the airflow through the duct or the area of the wind turbine to find the mechanical power that can be extracted.

The range of the air velocities within an air duct is [24]:

$$v_{\min} = 5 \text{ m/s}$$

$$v_{\max} = 11 \text{ m/s}$$

Referring to this table of common rectangular ducts [25], a relationship can be formed between fluid power and the duct size at velocity v_{min} . This is shown by the values in Table 17.

Table 17: Fluid power versus cross-sectional area for air at 5 m/s.

Width (mm)	Height (mm)										
	100	150	200	250	300	400	500	600	800	1000	1200
200	1.53	2.30	3.06	3.83	4.59	6.13	7.66	9.19	12.25	15.31	18.38
250	1.91	2.87	3.83	4.79	5.74	7.66	9.57	11.48	15.31	19.14	22.97
300	2.30	3.45	4.59	5.74	6.89	9.19	11.48	13.78	18.38	22.97	27.56
400	3.06	4.59	6.13	7.66	9.19	12.25	15.31	18.38	24.50	30.63	36.75
500	3.83	5.74	7.66	9.57	11.48	15.31	19.14	22.97	30.63	38.28	45.94
600	4.59	6.89	9.19	11.48	13.78	18.38	22.97	27.56	36.75	45.94	55.13
800	6.13	9.19	12.25	15.31	18.38	24.50	30.63	36.75	49.00	61.25	73.50
1000	7.66	11.48	15.31	19.14	22.97	30.63	38.28	45.94	61.25	76.56	91.88
1200	9.19	13.78	18.38	22.97	27.56	36.75	45.94	55.13	73.50	91.88	110.25
1400	10.72	16.08	21.44	26.80	32.16	42.88	53.59	64.31	85.75	107.19	128.63
1600	12.25	18.38	24.50	30.63	36.75	49.00	61.25	73.50	98.00	122.50	147.00
1800	13.78	20.67	27.56	34.45	41.34	55.13	68.91	82.69	110.25	137.81	165.38
2000	15.31	22.97	30.63	38.28	45.94	61.25	76.56	91.88	122.50	153.13	183.75

According to Betz's Law [12], at most 59.3% of the fluid's kinetic energy can be converted to mechanical energy. Thus, the maximum obtainable power by an ideal turbine the size of the air duct can be found by multiplying the fluid power with Betz's coefficient:

$$P_{\text{turbine, ideal}} = \frac{16}{27} \times P_{\text{fluid}}$$

This gives the range of values in Table 18.

Observe from Equation 4 that increasing the fluid's velocity v will give a cubic increase in the total power of the fluid.

Table 18: Maximum obtainable turbine power versus cross-sectional area at 5 m/s.

Width (mm)	Height (mm)										
	100	150	200	250	300	400	500	600	800	1000	1200
200	0.91	1.36	1.81	2.27	2.72	3.63	4.54	5.44	7.26	9.07	10.89
250	1.13	1.70	2.27	2.84	3.40	4.54	5.67	6.81	9.07	11.34	13.61
300	1.36	2.04	2.72	3.40	4.08	5.44	6.81	8.17	10.89	13.61	16.33
400	1.81	2.72	3.63	4.54	5.44	7.26	9.07	10.89	14.52	18.15	21.78
500	2.27	3.40	4.54	5.67	6.81	9.07	11.34	13.61	18.15	22.69	27.22
600	2.72	4.08	5.44	6.81	8.17	10.89	13.61	16.33	21.78	27.22	32.67
800	3.63	5.44	7.26	9.07	10.89	14.52	18.15	21.78	29.04	36.30	43.56
1000	4.54	6.81	9.07	11.34	13.61	18.15	22.69	27.22	36.30	45.37	54.44
1200	5.44	8.17	10.89	13.61	16.33	21.78	27.22	32.67	43.56	54.44	65.33
1400	6.35	9.53	12.70	15.88	19.06	25.41	31.76	38.11	50.81	63.52	76.22
1600	7.26	10.89	14.52	18.15	21.78	29.04	36.30	43.56	58.07	72.59	87.11
1800	8.17	12.25	16.33	20.42	24.50	32.67	40.83	49.00	65.33	81.67	98.00
2000	9.07	13.61	18.15	22.69	27.22	36.30	45.37	54.44	72.59	90.74	108.89

Appendix B. Battery life

From the input current column of Table 6, the mechatronic system (with all sensor devices enabled) will draw a current on average of:

$$I_{\text{effective}} = 50 + 150 + 2.5 + 32 + 16 + 20 = 270.5 \text{ mA} = 0.27 \text{ A}$$

When the system is at rest, the current load realistically is the current draw of the micro-controller:

$$I_{\text{rest}} = 20 \text{ mA} = 0.02 \text{ A}$$

The effective discharge current should not be more than 1/10 of the rated battery capacity [26]:

$$\begin{aligned} I_{\text{effective}} &= \frac{1}{10} \times Q \\ 0.27 &= \frac{1}{10} \times Q \\ \therefore Q &= 2.7 \text{ A} \end{aligned}$$

The battery's effective capacity is 2/3 of its rated capacity [26]:

$$\begin{aligned} Q_{\text{effective}} &= \frac{2}{3} \times Q \\ &= \frac{2}{3} \times 2.7 \\ \therefore Q_{\text{effective}} &= 1.8 \text{ Ah} \end{aligned}$$

Consider the battery life formula:

$$b = \frac{Q}{I} \tag{5}$$

Where:

- b (hr) is the battery life.
- Q (Ah) is the battery capacity.
- I (A) is the current load.

The battery life of the mechatronic system on average is:

$$\begin{aligned} b_{\text{load}} &= \frac{Q_{\text{effective}}}{I_{\text{effective}}} \\ &= \frac{1.8}{0.27} \\ \therefore b_{\text{load}} &= 6.66 \text{ hr} \end{aligned}$$

The battery life for current draw when the mechatronic system is at rest is:

$$\begin{aligned} b_{\text{rest}} &= \frac{Q_{\text{effective}}}{I_{\text{rest}}} \\ &= \frac{1.8}{0.02} \\ \therefore b_{\text{load}} &= 90 \text{ hr} \end{aligned}$$

Therefore, any rechargeable battery that is capable of supplying at least 7 V (to power any micro-controller) and with a capacity of at least 2.7 Ahr is desired.

Appendix C. Mechatronic system power

From the input current column of Table 6, the mechatronic system (with all sensor devices enabled) will draw a current on average of:

$$I_{\text{effective}} = 50 + 150 + 2.5 + 32 + 16 + 20 = 270.5 \text{ mA} = 0.27 \text{ A}$$

Consider the electrical power formula:

$$P = VI \quad (6)$$

Where:

- P (W) is the power.
- V (V) is the voltage.
- I (A) is the current.

Since the supply voltage is 7 V , the mechatronic system with sensor devices enabled will effectively have a power consumption of:

$$P_{\text{mechatronic}} = VI = 7 \times 0.27 = 1.89 \text{ W}$$

However, the power consumption of just the mechatronic system's essential devices i.e. the Arduino UNO and Arduino WiFi Shield is:

$$P_{\text{mechatronic, essential}} = VI = 7 \times (0.05 + 0.15) = 1.4 \text{ W}$$

Appendix D. Technical analysis and selection of the electric generator

The generalised operating windows of the two motor types are shown in Figure 15. It is evident that stepper motors have a much lower operating window from 500-1200 RPM as seen from the motor specifications in [27].

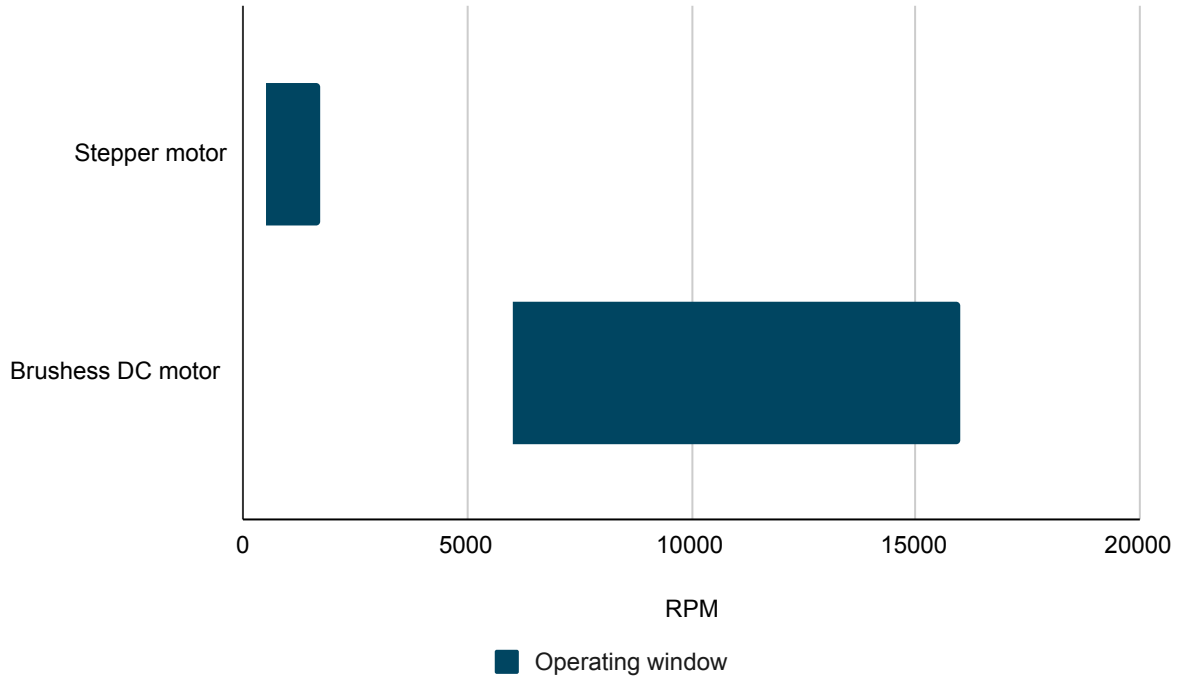


Figure 15: Operating window of a stepper motor [27] vs a brushless DC motor [28].

Due to the size and operating constraints of the electric generator, the smaller NEMA 11 stepper motor from [27] was chosen to be used in a motor generator configuration. The voltage output of the small-scale turbine design in [15] which also uses the NEMA 11, correlates to the RPM curve shown in Figure 16.

The wind turbine design from [15] was tested to produce 12 volts at 0.4 amps which gives:

$$\begin{aligned}
 P &= IV \\
 &= 12 \times 0.4 \\
 &= 4.8 \approx 5 \text{ watts}
 \end{aligned}$$

This is approximately the power that is required at minimum by the mechatronic system. Referring to Figure 16, this voltage is produced at ~1100 RPM at the motor shaft.

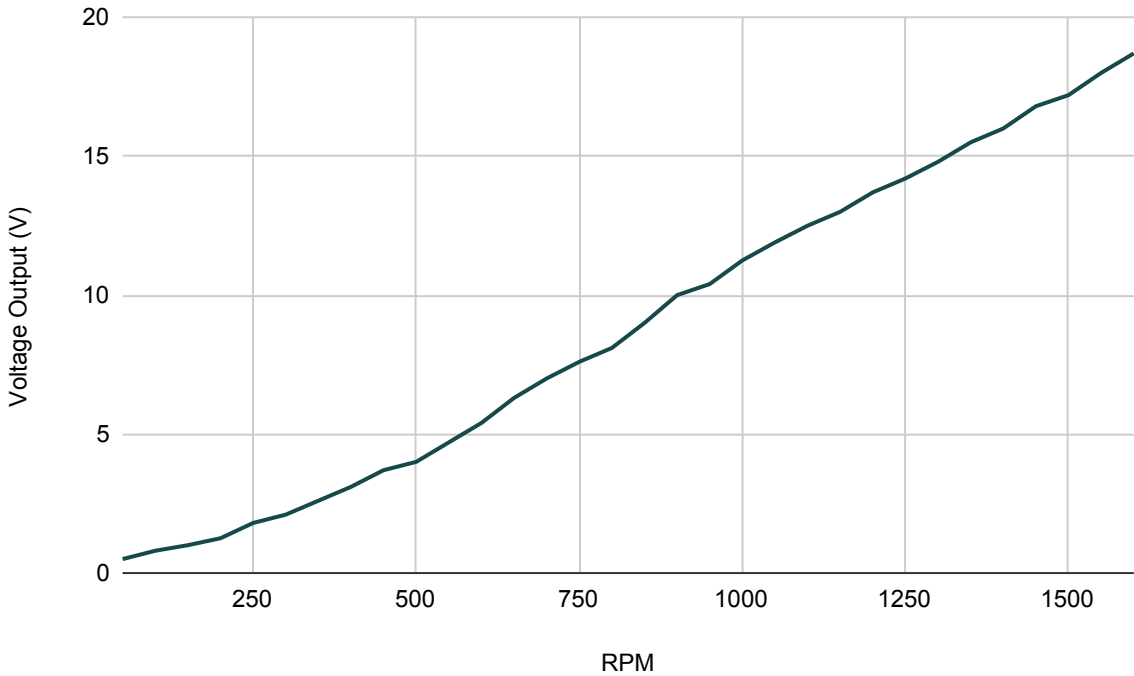


Figure 16: Voltage output of the NEMA-11 stepper motor vs RPM [27].

Alternating-current (AC) is produced by each phase of the NEMA 11 and needs to be rectified to be direct-current (DC). Along with a voltage regulator to smooth the current, it ensures that the electricity produced can be used by the system. The electrical diagram in Figure 17 shows how that can be achieved and follows the diagram shown in [15].

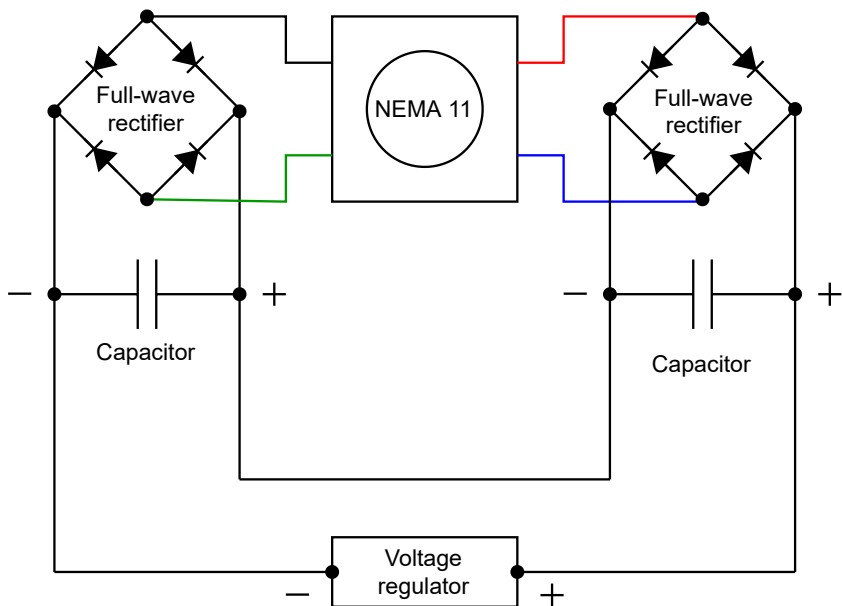


Figure 17: Electrical circuit diagram for the NEMA 11 motor-generator [15].

Appendix E. Technical design and analysis of the aerodynamic fairing

In fluid dynamics, when passing through a constriction, a fluid's velocity is increased while the static pressure is decreased as observed by Bernoulli's principle [16]. Thus, air velocity can be increased by using a funnel whilst maintaining the same flow rate:

$$Q = A_1 v_1 = A_2 v_2 \quad (7)$$

Where:

- Q (m^3/s) is the volumetric flow rate through the funnel.
- A_1 (m^2) is the cross-sectional area at the start of the funnel.
- v_1 (m/s) is the fluid velocity at the start of the funnel.
- A_2 (m^2) is the cross-sectional area at the end of the funnel.
- v_2 (m/s) is the fluid velocity at the end of the funnel.

To accelerate the incoming air by a factor of 2, the following ratio must be observed in Equation 7:

$$\frac{A_1}{A_2} = \frac{v_2}{v_1} = 2$$

Since $A_1 = w_1 \times h_1$ and $A_2 = w_2 \times h_2$:

$$\frac{w_1 \times h_1}{w_2 \times h_2} = 2$$

Let the height of the funnel start be:

$$h_1 = 0.2 \text{ m}$$

The height of the turbine blade is the height of the funnel end:

$$h_2 = 0.175 \text{ m}$$

The width of the funnel start can be determined by the diameter of the base of the assembly (refer to Figure 18).

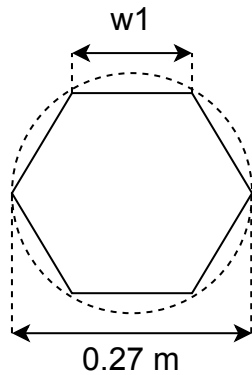


Figure 18: Funnel opening diagram.

$$w_1 = \frac{0.27}{2} = 0.135 \text{ m}$$

Round down w_1 to account for the thickness of the material:

$$w_1 = 0.13 \text{ m}$$

Therefore w_2 can be calculated:

$$w_2 = \frac{w_1 \times h_1}{2 \times h_2} = \frac{0.13 \times 0.2}{2 \times 0.175} = 0.074 \text{ m}$$

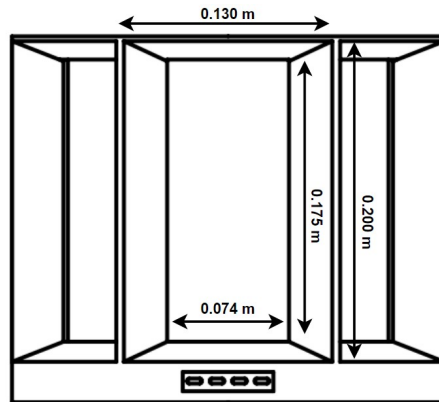


Figure 19: Dimensions of air accelerating funnel.

The range of fluid velocity after acceleration is therefore:

$$v_{\min} = 10 \text{ m/s}$$

$$v_{\max} = 22 \text{ m/s}$$

Appendix F. Change in fluid power

The fluid force can be derived in terms of the fluid velocity and area:

$$\begin{aligned} F &= \frac{d}{dt}(mv) \\ &= \frac{dm}{dt}v \\ \therefore F &= \rho Av^2 \end{aligned}$$

The power can then be derived from the force of the fluid and velocity:

$$\begin{aligned} P &= Fv \\ &= \rho Av^2 \times v \\ \therefore P &= \rho Av^3 \end{aligned}$$

Therefore, the change in power can be determined by considering Equation 7 (the law of conservation of mechanical energy is preserved since the flow rate is constant):

$$\Delta P = P_2 - P_1 = \rho (A_2 v_2^3 - A_1 v_1^3)$$

Since v^3 changes by a cubic factor versus a linear factor in A , it can be assumed that changes in fluid velocity is more significant than changes in area. Therefore, the change in power is strongly dependent on change in fluid velocity.

Appendix G. Flettner ventilator



Figure 20: An exploded view of the Flettner TXC-2™ ventilator [29]

Appendix H. Technical analysis of turbine output power

It has been determined that the turbine must be made to fit within these dimensions:

$$\text{diameter} = 0.2 \text{ m}$$

$$\text{height} = 0.175 \text{ m}$$

So, the radius of the blade R will be made to be 0.1 metres and the height h will be 0.175 metres.

Consider the coefficient of power formula for a turbine:

$$C_p = \frac{P_{\text{out}}}{P_{\text{fluid}}} \quad (8)$$

Where:

- C_p (dimensionless) is the power coefficient of the turbine.
- P_{out} (W) is the output power of the turbine.
- P_{fluid} (W) is the power of the fluid.

The peak power coefficient of the selected blade was experimentally obtained from [19] as:

$$C_p = 0.25$$

The vertical cross-sectional area of the turbine is:

$$\begin{aligned} A &= h \times 2R \\ &= 0.175 \times 0.2 \\ &= 0.035 \text{ m}^2 \end{aligned}$$

The range of wind speed for turbine operation is:

$$v = [10, 22] \text{ m/s}$$

For the minimum wind speed, the minimum output power can be calculated by using Equation 4 and Equation 8:

$$\begin{aligned} C_p &= \frac{P_{\text{out}, \text{min}}}{\frac{1}{2}\rho Av^3} \\ 0.25 &= \frac{P_{\text{out}, \text{min}}}{\frac{1}{2} \times 1.225 \times 0.035 \times 10^3} \\ \therefore P_{\text{out}, \text{min}} &= 5.56 \text{ W} \end{aligned}$$

For the maximum wind speed, the maximum output power can be calculated by using using Equation 4 and Equation 8:

$$C_p = \frac{P_{\text{out, max}}}{\frac{1}{2}\rho A v^3}$$

$$0.25 = \frac{P_{\text{out, max}}}{\frac{1}{2} \times 1.225 \times 0.035 \times 22^3}$$

$$\therefore P_{\text{out, max}} = 57.07 \text{ W}$$

The TSR is a ratio between the tangential blade-tip velocity over the air velocity:

$$\lambda = \frac{\text{blade tip velocity}}{\text{air velocity}}$$

$$= \frac{\omega R}{v} \quad (9)$$

Where:

- λ (dimensionless) is the tip speed ratio.
- ω (rad/s) is the turbine angular velocity.
- R (m) is the radius of the turbine.
- v (m/s) is the air velocity.

For the twisted two-bladed turbine design at its peak efficiency with a power coefficient of 0.25, the tip speed ratio is:

$$\lambda = 0.55$$

Rearranging Equation 9 to find ω , gives:

$$\omega = \frac{\lambda v}{R} \quad (10)$$

Therefore, minimum turbine rotational velocity using Equation 10 is:

$$\omega_{\min} = \frac{\lambda v_{\min}}{R}$$

$$= \frac{0.55 \times 10}{0.1}$$

$$= 55 \text{ rad/s (525 RPM)}$$

Also, maximum turbine rotational velocity using Equation 10 is:

$$\begin{aligned}\omega_{\max} &= \frac{\lambda v_{\max}}{R} \\ &= \frac{0.55 \times 22}{0.1} \\ &= 121 \text{ rad/s (1155 RPM)}\end{aligned}$$

The relationship between output power and torque is:

$$P = Q\omega \quad (11)$$

Where:

- P (W) is the turbine power.
- Q (Nm) is the turbine torque.
- ω (rad/s) is the turbine rotational velocity.

The minimum turbine torque using Equation 11 is therefore:

$$\begin{aligned}P_{\min} &= Q_{\min}\omega_{\min} \\ 5.56 &= Q_{\min} \times 55 \\ \therefore Q_{\min} &= 0.101 \text{ Nm}\end{aligned}$$

Also, the maximum turbine torque using Equation 11 is:

$$\begin{aligned}P_{\max} &= Q_{\max}\omega_{\max} \\ 57.07 &= Q_{\max} \times 121 \\ \therefore Q_{\max} &= 0.472 \text{ Nm}\end{aligned}$$

Appendix I. Technical analysis and design of the drive train

The aim of this belt drive system is to provide the required RPMs to the motor at the air velocity v_{min} , such that the minimum power requirements are always met. The design of the flat belt drive follow methods outlined in [30].

The required gear ratio can be determined as:

$$\begin{aligned} \text{ratio} &= \frac{\omega_{\text{output}}}{\omega_{\text{input}}} \\ &= \frac{1100}{525} \\ &= 2.09 \approx 2 \end{aligned}$$

The distance from the centre of the turbine pulley to the edge of the generator pulley should be made to be less than half the diameter of the base which is 128.94 mm. This is to ensure that the drive system can be fitted within the base of the turbine. Figure 21 shows the required dimensions of the flat belt drive system to be 100mm, which satisfies the size constraint.

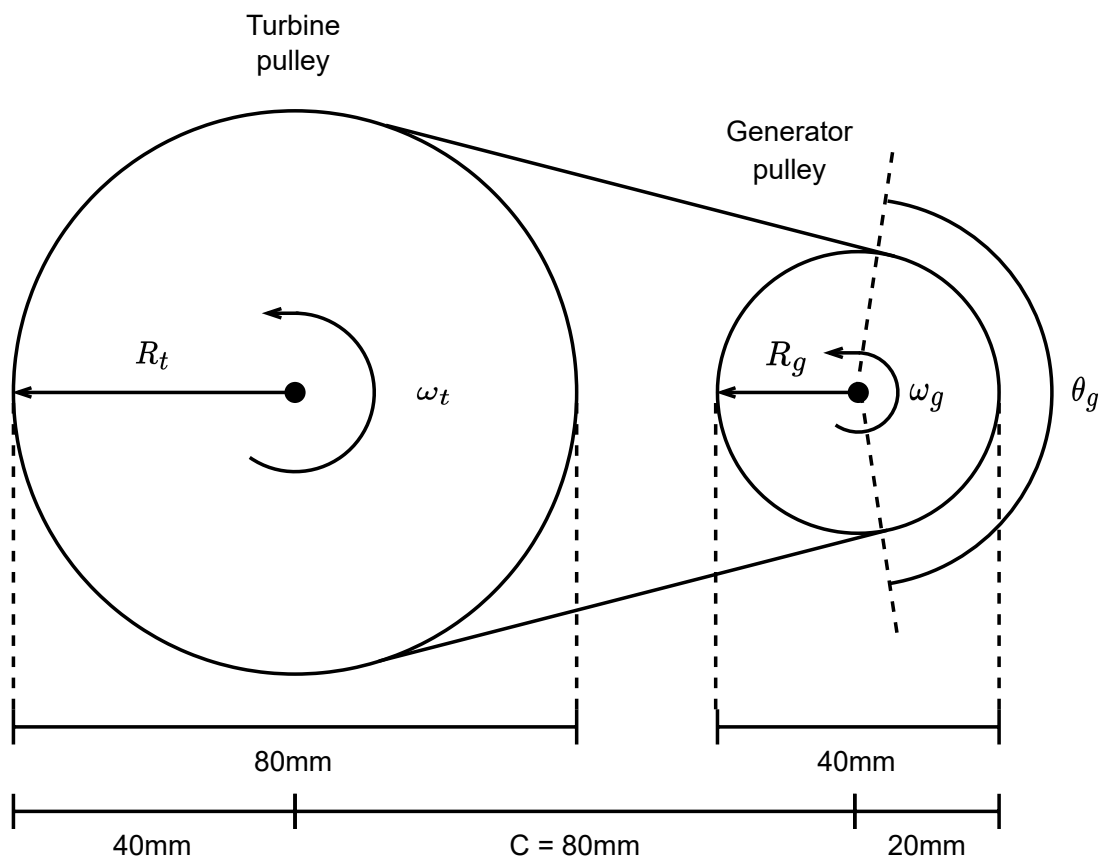


Figure 21: Dimensions of the flat-belt pulley drive system.

The belt length is therefore calculated as:

$$\begin{aligned}
 L &= 2C + \pi(R_t + R_g) + \frac{(R_t - R_g)^2}{C} \\
 &= 2 \times 0.08 + \pi(0.04 + 0.02) + \frac{(0.04 - 0.02)^2}{0.08} \\
 &= 0.3535 \text{ m}
 \end{aligned}$$

No slippage is expected since the turbine will not have any abrupt changes in its rotational velocity and the experienced load is not significant. So the belt speed can be determined as:

$$v_b = R_t \omega_t = R_g \omega_g = 2.2 \text{ m/s}$$

This is significantly under the maximum velocity specified under [30] and is satisfactory.

Another important factor is the angle of wrap on the smaller pulley defined as θ_g to be greater than 120 degrees [30]. This is to ensure that slippage is less likely to occur and can be found by:

$$\begin{aligned}
 \theta_g &= \pi - 2\sin^{-1} \left(\frac{R_t - R_g}{C} \right) \\
 &= \pi - 2\sin^{-1} \left(\frac{0.04 - 0.02}{0.08} \right) \\
 &= 2.6362 \text{ rad } (151^\circ)
 \end{aligned}$$

This clearly also satisfies the angle of wrap condition on the smaller generator pulley.

Therefore, for a small scale drive train, the design parameters have been satisfied as in [30].

The power transmitted and torque at each pulley can be calculated as:

$$P_{transmitted} = (F_1 - F_2) \cdot v_b \quad (12)$$

$$T = (F_1 - F_2) \cdot R \quad (13)$$

It was calculated in Appendix H that the torque and angular velocity values are:

$$\omega_{\min} = 55 \text{ rad/s}$$

$$Q_{\min} = 0.101 \text{ Nm}$$

$$\omega_{\max} = 121 \text{ rad/s}$$

$$Q_{\max} = 0.472 \text{ Nm}$$

The minimum transmitted power in Equation 12 can be found by substituting Equation 13:

$$\begin{aligned} P_{\text{transmitted, min}} &= \frac{T_{t,\min}}{R_t} \cdot v_{b,\min} \\ &= \frac{0.101}{0.04} \times 2.2 \\ &= 5.555 \text{ W} \end{aligned}$$

Similarly, for the maximum transmitted power:

$$\begin{aligned} P_{\text{transmitted, max}} &= \frac{T_{t,\max}}{R_t} \cdot v_{b,\max} \\ &= \frac{0.472}{0.04} \times 4.84 \\ &= 57.112 \text{ W} \end{aligned}$$

Also, using Equation 13 and substituting Equation 12, the minimum torque at the generator pulley can be calculated:

$$\begin{aligned} T_{g,\min} &= \frac{P_{\text{transmitted, min}}}{v_{b,\min}} \cdot R_g \\ &= \frac{5.555}{2.2} \times 0.02 \\ &= 0.0505 \text{ Nm} \end{aligned}$$

Likewise, the maximum torque can be found as:

$$\begin{aligned} T_{g,\max} &= \frac{P_{\text{transmitted, max}}}{v_{b,\max}} \cdot R_g \\ &= \frac{57.1112}{4.84} \times 0.02 \\ &= 0.2360 \text{ Nm} \end{aligned}$$

The minimum torque at the generator $T_{g,\min}$, is greater than the starting torque required by the NEMA 11 motor in [27]. Therefore, the drive train is able to start the generator at the minimum wind speeds. Also, it is reasonable for the generator to produce less than the transferred power due to efficiency losses.

Appendix J. Factor of safety

Factor of safety (FOS) is a significant design parameter to ensure the safety and reliability of the turbine. FOS is the factor of increase from an allowable load to a failure load:

$$FOS = \frac{\text{failure load}}{\text{allowable load}} \quad (14)$$

Variables influencing desired FOS [31] are:

- Load.
- Risk analysis of failure.
- Engineering model confidence.
- Material selection confidence.

Table 19 was developed to methodically identify appropriate factors of safety with respect to the above list of influencing variables.

Table 19: Factor of safety measurement guide.

Confidence Level	Factor of Safety Increase
Certain	0.0
Very High	0.1
High	0.2
Moderately High	0.3
Moderate	0.4
Moderately Low	0.5
Low	0.6
Very Low	0.7
None	0.8

With consideration of the FOS measurement guide, the adjusted factor of safety for each variable is tabulated in Table 20:

Table 20: Turbine factor of safety variables.

Variable	Confidence Level	Factor of Safety Increase	Comment
Load	High	0.2	Loads make some minor assumptions.
Risk analysis of failure	Very High	0.1	Turbine is not intended to operate within human-occupied areas.
Engineering model confidence	Moderately Low	0.5	Models makes major assumptions.
Material selection confidence	Moderately Low	0.5	There exists a wide margin on quality of ABS.

The suggested factor of safety for turbines [32] is 2. Therefore, with consideration of the adjusted factors of safety in Table 20, the final minimum factor of safety is:

$$FOS_{\min} = 2 + 0.2 + 0.1 + 0.5 + 0.5 = 3.3$$

Appendix K. Finite element analysis of axial spline loads

Let the Young's modulus of ABS be [33]:

$$E_{\text{ABS}} = 1400 \text{ MPa}$$

There are no lift forces contributing to the axial load since the turbine blade is drag-based. Therefore, the axial force acting on the spline is simply the weight of the rotor components itself i.e.

$$F_{\text{axial, max}} = m_{\text{turbine + shaft}} \times g = 0.73 \text{ N}$$

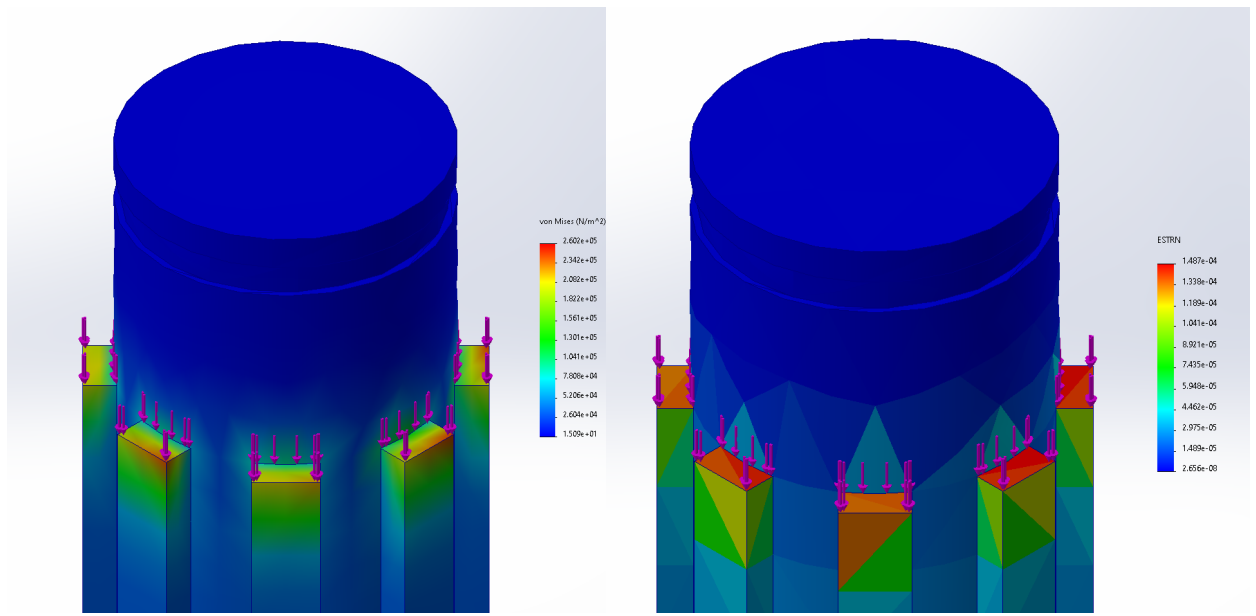
Let the axial force applied on the turbine be:

$$F_{\text{axial, safe}} = 3 \text{ N}$$

This gives a factor of safety of:

$$FOS = \frac{F_{\text{axial, safe}}}{F_{\text{axial, max}}} = \frac{3}{0.73} = 4.11$$

FEA was performed for the axial load on the shoulder of the spline as shown in Figure 22 below.



(a) Stress plot of 10 mm OD shaft spline. (b) Strain plot of 10 mm OD shaft spline.

Figure 22: FEA of 10 mm OD shaft spline.

Figure 22 shows the region of greatest stress and strain as red which are respectively:

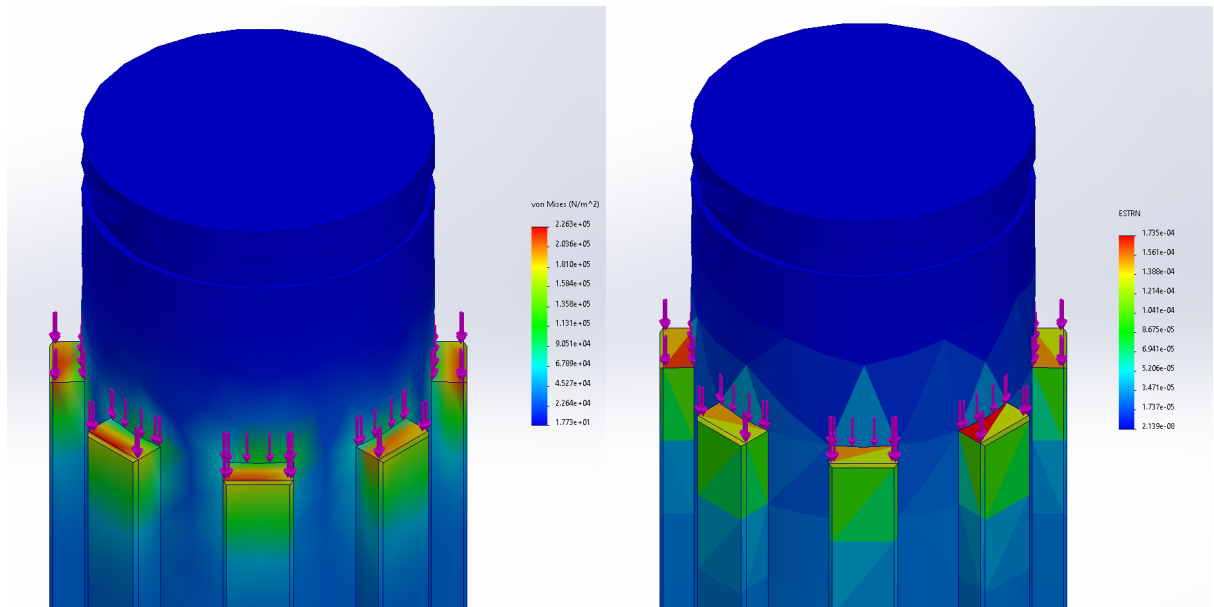
$$\sigma = 2.602 \times 10^5 \text{ Pa}$$

$$\epsilon = 1.407 \times 10^{-4}$$

σ and ϵ are substituted into the modulus of elasticity equation (i.e. Equation 1) to yield:

$$\lambda = \frac{2.602 \times 10^5}{1.407 \times 10^{-4}} = 1849 \text{ MPa} > E_{\text{ABS}}$$

The modulus of elasticity is greater than the Young's modulus of ABS, therefore the part will permanently deform under the given axial load of 3 N. It is clear from the FEA that the most stress is applied on the corner of the spline. A chamfer is applied and the FEA was performed again as shown in Figure 23 below.



(a) Stress plot of 10 mm OD shaft spline. (b) Strain plot of 10 mm OD shaft spline.

Figure 23: FEA of 10 mm OD shaft spline with chamfer.

Figure 23 shows the modulus of elasticity of the spline with a chamfer under an axial load to be:

$$\lambda = \frac{2.263 \times 10^5}{1.735 \times 10^{-4}} = 1304 \text{ MPa} < E_{\text{ABS}}$$

Appendix L. Finite element analysis of rotational spline loads

The force of the fluid acting on the turbine is obtained from considering the maximum power and velocity of the fluid:

$$\begin{aligned} P_{\text{fluid, max}} &= F_{\text{fluid, max}} v_{\text{fluid, max}} \\ 57.07 &= F_{\text{fluid, max}} \times 22 \\ \therefore F_{\text{fluid, max}} &= 2.59 \text{ N} \end{aligned}$$

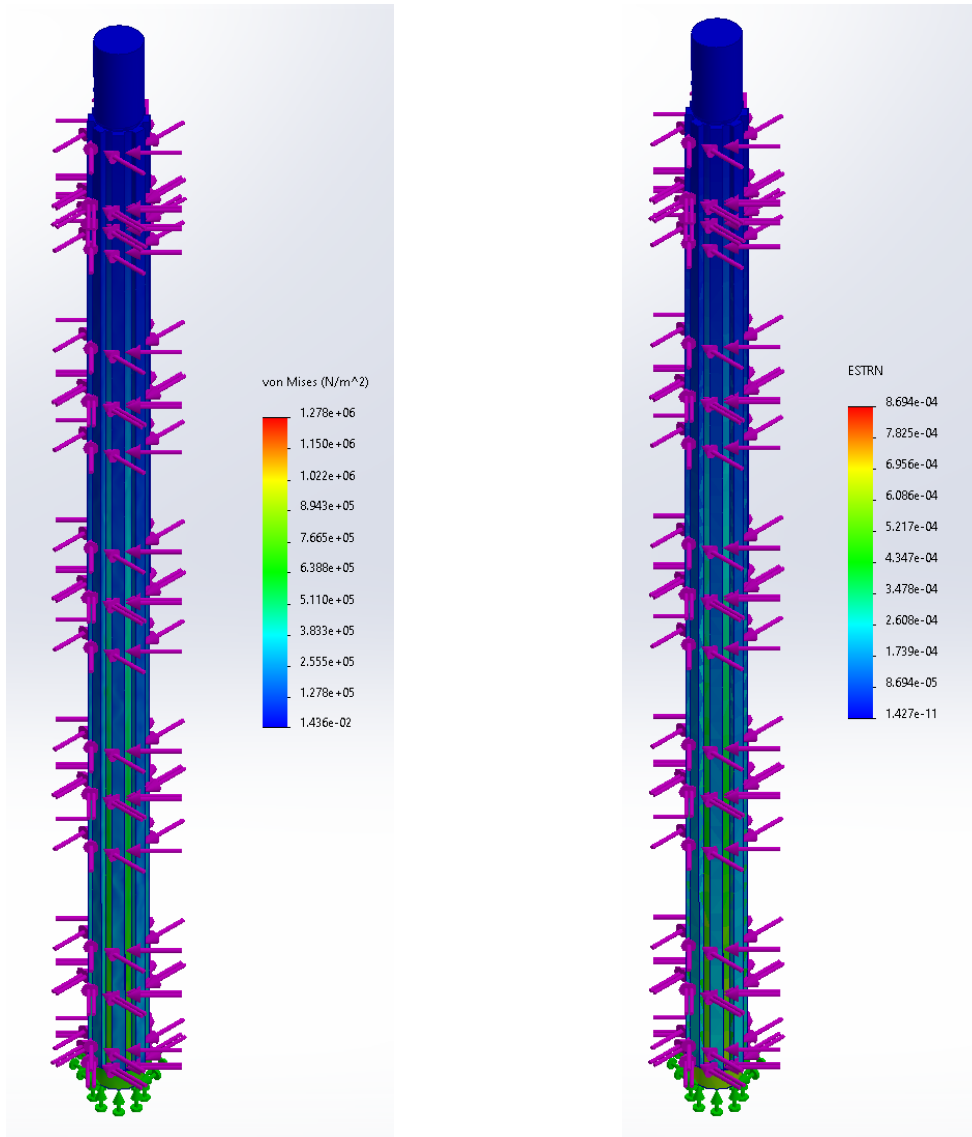
The rotational force acting on the spline is the force of the fluid impacting the blade. Let the rotational force applied on the turbine be:

$$F_{\text{fluid, safe}} = 10 \text{ N}$$

This gives a factor of safety (justified in Appendix J) of:

$$FOS = \frac{F_{\text{fluid, safe}}}{F_{\text{fluid, max}}} = \frac{10}{2.59} = 3.86$$

FEA was performed for the rotational load on the spline as shown in Figure 24 below.



(a) Stress plot of 8 mm OD shaft.

(b) Strain plot of 8 mm OD shaft.

Figure 24: FEA of 8 mm OD shaft.

Figure 24 shows the region of greatest stress and strain as red which are respectively:

$$\sigma = 1.278 \times 10^6 \text{ Pa}$$

$$\epsilon = 8.694 \times 10^{-4}$$

σ and ϵ are substituted into the modulus of elasticity equation (i.e. Equation 1) to yield:

$$\lambda = \frac{1.278 \times 10^6}{8.694 \times 10^{-4}} = 1467 \text{ MPa} > E_{\text{ABS}}$$

The modulus of elasticity is greater than the Young's modulus of ABS, therefore the part will permanently deform under the given rotational load of 10 N. The max stress

is applied at the circlip groove however the groove cannot be modified since the circlip mates with this groove - the diameter of the shaft was increased instead. The FEA was performed again as shown in Figure 23 below.

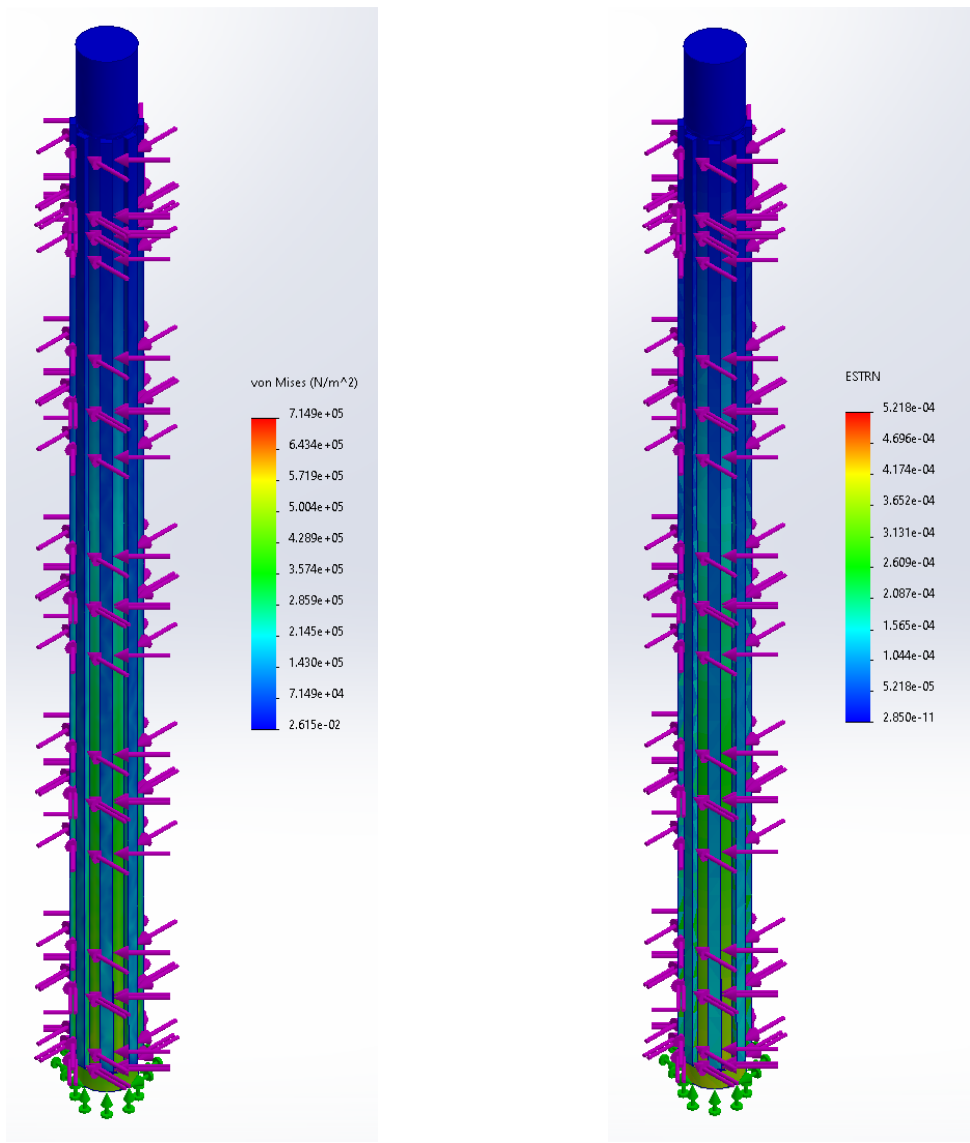


Figure 25: FEA of 10 mm OD shaft.

Figure 25 shows the modulus of elasticity for a 10 mm outer diameter shaft under rotational load is:

$$\lambda = \frac{7.149 \times 10^5}{5.218 \times 10^{-4}} = 1370 \text{ MPa} < E_{\text{ABS}}$$

Appendix M. Circlip calculation

Assume the circlip is axially loaded with only the weight of the turbine:

$$\begin{aligned} F_{\text{axial}} &= m_{\text{turbine}} \times g \\ &= 5 \times 9.81 \\ &= 49.05 \text{ N} \end{aligned}$$

Considering the case where the circlip is axially-loaded (Figure 11a), the FOS of the circlip is given in the form of Equation 14 [34]:

$$K_a = \frac{DTS_S\pi}{F_{\text{axial}}} \quad (15)$$

Where:

- K_a is the FOS of an axially-loaded circlip.
- D (m) is the shaft diameter.
- T (m) is the circlip thickness.
- S_S (Pa) is the shear strength of the circlip material.
- F_{axial} (N) is the axial load on the circlip.

BS3673 requires the shaft diameter to be 10 mm and the circlip thickness to be 1 mm . The shear strength of the circlip (i.e. steel) is 340 MPa [35]. Substituting these values into Equation 15 yields:

$$\begin{aligned} K_a &= \frac{DTS_S\pi}{F_{\text{axial}}} \\ &= \frac{10 \times 10^{-3} \times 1 \times 10^{-3} \times 340 \times 10^6 \times \pi}{49.05} \\ &= 218 \end{aligned}$$

Since the factor of safety is significantly greater than 3.3 (Appendix J), the circlip will not fail in this case.

Considering the case where the circlip groove is axially-loaded (Figure 11b), the FOS of the groove is given in the form of Equation 14 [34]:

$$K_b = \frac{DdS_Y\pi}{F_{\text{axial}}} \quad (16)$$

Where:

- K_b is the FOS of an axially-loaded circlip groove.
- D (m) is the shaft diameter.
- d (m) is the groove depth.
- S_Y (Pa) is the yield strength of the circlip groove material.
- F_{axial} (N) is the axial load on the circlip groove.

BS3673 requires the groove depth to be 0.2 mm . The yield strength of the material (i.e. ABS) is 40 MPa [33]. Substituting these values into Equation 16 yields:

$$\begin{aligned} K_b &= \frac{DdS_Y\pi}{F_{\text{axial}}} \\ &= \frac{10 \times 10^{-3} \times 0.2 \times 10^{-3} \times 40 \times 10^6 \times \pi}{49.05} \\ &= 5.12 \end{aligned}$$

Since the factor of safety is greater than 3.3 (Appendix J), the circlip groove will not fail in this case.

Appendix N. Finite element analysis for blade optimisation

The force impacting the blade is the same fluid force from Appendix L:

$$F_{\text{fluid, safe}} = 10 \text{ N for a factor of safety of 3.86}$$

FEA was performed for the fluid force on the blade as shown in Figure 26 below.

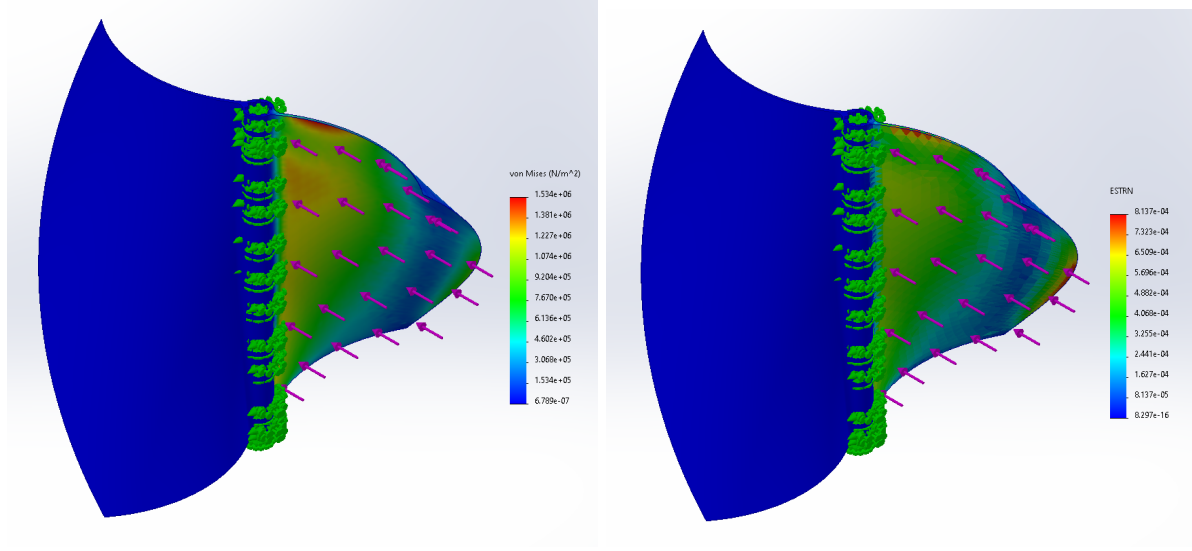


Figure 26: FEA of 2 mm thick turbine blade.

Figure 26 shows the region of greatest stress and strain as red which are respectively:

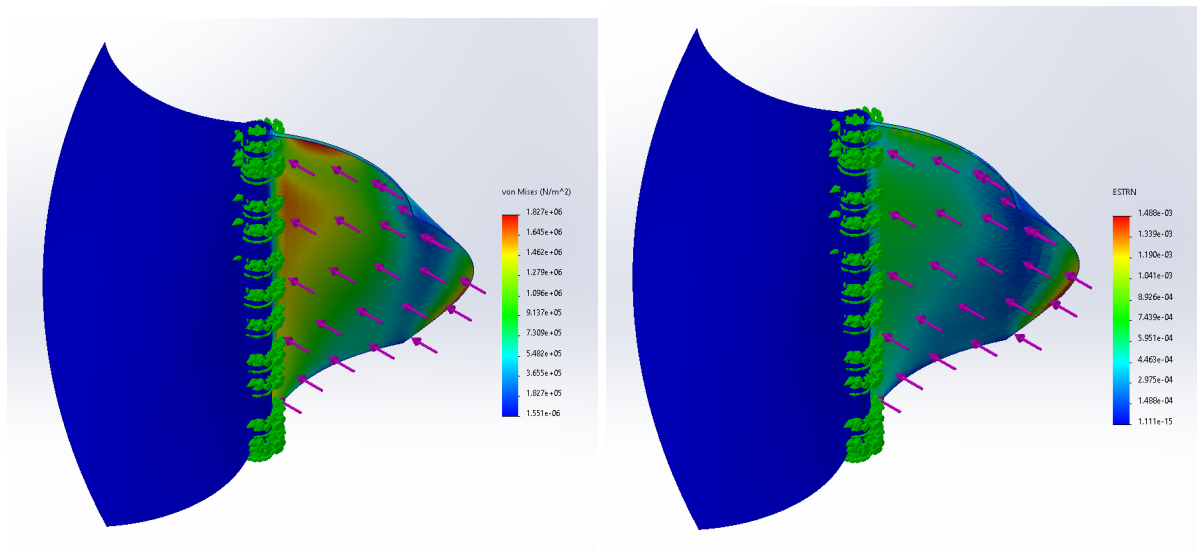
$$\sigma = 1.534 \times 10^6 \text{ Pa}$$

$$\epsilon = 8.137 \times 10^{-4}$$

σ and ϵ are substituted into the modulus of elasticity equation (i.e. Equation 1) to yield:

$$\lambda = \frac{1.534 \times 10^6}{8.137 \times 10^{-4}} = 1885 \text{ MPa} > E_{\text{ABS}}$$

The modulus of elasticity is greater than the Young's modulus of ABS, therefore the part will permanently deform under the fluid load of 10 N. The max stress is applied along the edge of the fillet between the blade and the shaft. Therefore, the blade thickness is increased and the FEA was performed again as shown in Figure 27 below.



(a) Stress plot of 3 mm thick turbine blade. (b) Strain plot of 3 mm thick turbine blade.

Figure 27: FEA of 3 mm thick turbine blade.

Figure 27 shows the modulus of elasticity for a turbine blade with a base width of 3 mm is:

$$\lambda = \frac{1.827 \times 10^6}{1.488 \times 10^{-3}} = 1228 \text{ MPa} < E_{\text{ABS}}$$

The final cross-sectional sketch of the turbine blade is shown in Figure 28 below.

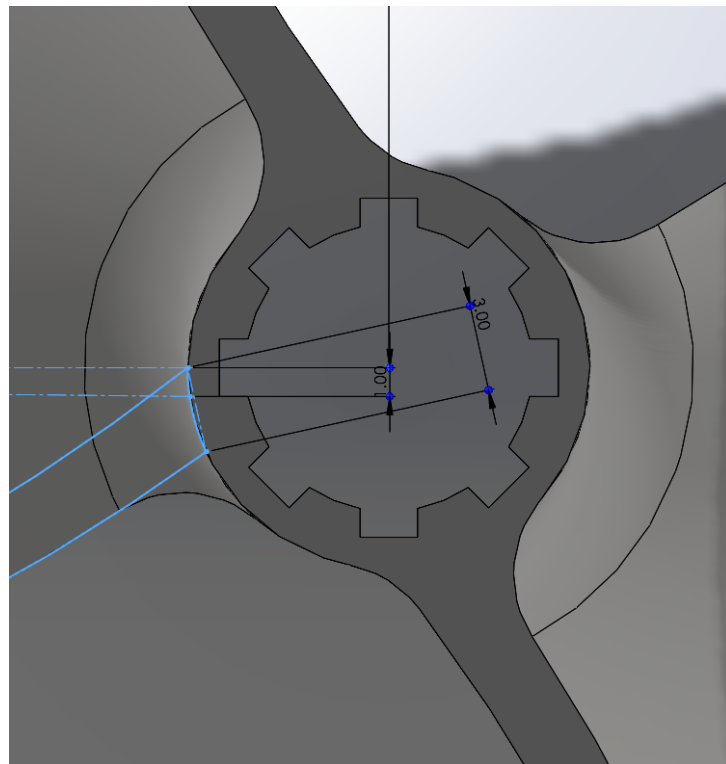


Figure 28: Sketch of turbine blade.

Appendix O. Bearing selection

To consider the suitability of a bearing, the equivalent dynamic bearing load is calculated as:

$$P = xF_r + yF_a \quad (17)$$

Where:

- x is the radial load factor.
- y is the axial load factor.
- F_r (N) is the actual radial bearing load.
- F_a (N) is the actual axial bearing load.

For a deep groove ball bearing type, the load factors are:

$$\begin{aligned} x &= 1, \quad y = 0 \text{ for } \frac{F_a}{F_r} \leq 0.5 \\ x &= 0.56, \quad y = [1, 2] \text{ for } \frac{F_a}{F_r} > 0.5 \end{aligned}$$

The actual radial bearing load (at worst) is the torque transferred from the turbine:

$$\begin{aligned} F_r &= \frac{\tau_{\text{turbine}}}{r_{\text{bearing}}} \\ &= \frac{0.472}{19 \times 10^{-3}} \\ &= 24.84 \text{ N} \end{aligned}$$

The actual axial bearing load is theoretically the rotor weight (because the turbine is drag-based and ideally no lift is generated):

$$\begin{aligned} F_a &= m_{\text{blade + shaft}} \times g \\ &= (56.52 + 17.51) \times 10^{-3} \times 9.81 \\ &= 0.73 \text{ N} \end{aligned}$$

The axial load to radial load ratio is:

$$\frac{F_a}{F_r} = \frac{0.73}{24.84} \approx 0.03$$

Therefore, the selected load factors are:

$$x = 1, \quad y = 0$$

F_r and F_a can then be substituted into Equation 17 to yield the equivalent dynamic bearing load:

$$\begin{aligned} P &= xF_r + yF_a \\ &= 1 \times 24.84 + 0 \times 0.73 \\ &= 24.84 \text{ N} \end{aligned}$$

Consider the bearing life:

$$L_{10} = \left(\frac{C}{P} \right)^a$$

Where:

- L (10^6 revolutions) is the bearing life in number of revolutions.
- C (N) is the dynamic load rating.
- P (N) is the equivalent dynamic load rating.
- a (dimensionless) is the bearing type factor.

For the 6800-2RS [36], the bearing life is:

$$\begin{aligned} L_{10} &= \left(\frac{C_{6800-2RS}}{P} \right)^a \\ &= \left(\frac{585}{24.84} \right)^3 \\ &= 13062 \times 10^6 \text{ revolutions} \end{aligned}$$

To calculate the bearing life in hours:

$$L_{10h} = \frac{10^6}{60\omega} L_{10}$$

Where:

- L_{10h} (hr) is the bearing life in hours.
- ω (RPM) is the rotational speed.
- L_{10} (10^6 revolutions) is the bearing life in number of revolutions.

$$\begin{aligned} L_{10h} &= \frac{10^6}{60\omega} L_{10} \\ &= \frac{10^6}{60 \times 577.7} \times 13062 \\ &= 376839 \text{ hr} \\ &\approx 43 \text{ years} \end{aligned}$$

Appendix P. Bolt selection

The threaded insert is assumed to act like a nut.

To consider the suitability of a bolt, the load due to weight is calculated as:

$$\begin{aligned}F &= ma \\&= 5 \times 9.81 \\&= 49.05 \text{ N downwards}\end{aligned}$$

Where:

- m (kg) is the mass of the system.
- a (ms^{-1}) is the acceleration due to gravity.

To ensure that the screw will fail before the thread strips, the minimum length of engagement between the female and male threads is calculated as:

$$L_{e(\min)} = \frac{2A_t}{0.5\pi d_p} \quad (18)$$

Where:

- D (mm) is the basic diameter of the bolt.
- p (mm) is the bolt thread pitch.
- L_e (mm) is the length of thread engagement.
- L (mm) is the length of the bolt.
- A_t (mm^2) is the bolt thread tensile stress area.
- d_p (mm) is the pitch circle diameter of the thread.

The tensile stress area of an M3 x 0.5 bolt is calculated as:

$$\begin{aligned}A_t &= \frac{\pi}{4}(D - 0.938194p)^2 \\&= \frac{\pi}{4}(3 - 0.938194(0.5))^2 \\&= 5.03 \text{ mm}^2\end{aligned}$$

The pitch circle diameter of the thread is calculated as:

$$\begin{aligned}d_p &= (D - 0.64952p) \\&= (3 - 0.64952(0.5)) \\&= 2.675 \text{ mm}\end{aligned}$$

A_t and d_p can then be substituted into Equation 18 to yield the minimum length of engagement:

$$\begin{aligned} L_{e(min)} &= \frac{2A_t}{0.5\pi d_p} \\ &= \frac{2(5.03)}{0.5\pi \times 2.675} \\ &= 2.39 \text{ mm} \end{aligned}$$

The total necessary length of the bolt must take into account the length from the bolt head to the threaded insert, the minimum length of engagement and the length of three threads. This is calculated as:

$$\begin{aligned} L &= 2 + 2.39 + 3 \times 0.5 \\ &= 5.89 \text{ mm} \end{aligned}$$

Therefore, a 6 mm long bolt is suitable.

The load factor of a lid is calculated as:

$$n_L = \frac{S_p A_t - F_i}{C(P/N)} \quad (19)$$

Where:

- S_p (MPa) is the proof strength on the bolt.
- A_t (mm^2) is the bolt thread tensile stress area.
- F_i (N) is the preload on the bolt.
- C is the joint constant on the bolt.
- P (N) is the load on the bolts.
- N is the number of bolts.

The proof load for a Grade 4.8 bolt is calculated as:

$$\begin{aligned} F_p &= S_p \times A_t \\ &= 310 \times 5.03 \\ &= 1559.3 \text{ N} \end{aligned}$$

For reused connections (i.e. the fastener is detachable) the preload is calculated as:

$$\begin{aligned} F_i &= 0.75F_p \\ &= 0.75 \times 1559.3 \\ &= 1169.48 \text{ N} \end{aligned}$$

The joint constant can be calculated as:

$$C = \frac{k_b}{k_b + k_m} \quad (20)$$

Where:

- k_b (N/mm) is the bolt stiffness.
- k_m (N/mm) is the material stiffness.

The bolt stiffness is calculated as:

$$\begin{aligned} k_b &= \frac{A_t E}{L} \\ &= \frac{5.03 \times 180 \times 10^3}{6} \\ &= 150.9 \times 10^3 \text{ N/mm} \end{aligned}$$

Where:

- A_t (mm^2) is the bolt thread tensile stress area.
- E (MPa) is Young's modulus.
- L (mm) is the length of the bolt.

The member stiffness is calculated as:

$$k_m = \frac{\pi E d \tan \alpha}{\ln \frac{(2t \tan \alpha + D + d)(D + d)}{(2t \tan \alpha + D + d)(D - d)}} \quad (21)$$

Where:

- E (MPa) is Young's Modulus.
- t (mm) is the member thickness.
- d (mm) is the diameter of the bolt.
- D (mm) is the diameter of the bolt head pressing into the member.
- α ($degrees$) uses the common assumption that it is equal to 30.

Using equation 21, the member stiffness at the top frustum is calculated as:

$$\begin{aligned} k_{top} &= \frac{\pi E d \tan \alpha}{\ln \frac{(2t \tan \alpha + D + d)(D + d)}{(2t \tan \alpha + D + d)(D - d)}} \\ &= \frac{\pi (180 \times 10^3) (3) \tan \alpha}{\ln \frac{(2(2) \tan \alpha + 5.5 + 3)(5.5 + 3)}{(2(2) \tan \alpha + 5.5 + 3)(5.5 - 3)}} \\ &= 2.366 \times 10^6 \text{ N/mm} \end{aligned}$$

Similarly, the member stiffness at the bottom frustum is calculated as:

$$k_{bottom} = \frac{\pi(180 \times 10^3)(3) \tan \alpha}{\ln \frac{(2(3) \tan \alpha + 8 + 3)(8 + 3)}{(2(3) \tan \alpha + 8 + 3)(8 - 3)}} \\ = 3.877 \times 10^6 \text{ N/mm}$$

The total member stiffness is calculated as:

$$\frac{1}{k_m} = \frac{1}{k_{top}} + \frac{1}{k_{bottom}} \\ = \frac{1}{2.366 \times 10^6} + \frac{1}{3.877 \times 10^6} \\ k_m = 1.469 \times 10^6$$

k_b and k_m can then be substituted into Equation 20 to yield the joint constant:

$$C = \frac{k_b}{k_b + k_m} \\ = \frac{150.9 \times 10^3}{150.9 \times 10^3 + 1.469 \times 10^6} \\ = 0.0931$$

S_p , A_t , F_i , C, P and N can then be substituted into Equation 19 to yield the load factor:

$$n_L = \frac{S_p A_t - F_i}{C(P/N)} \\ = \frac{310 \times 5.03 - 1169.48}{0.0931(\frac{49.05}{4})} \\ = 341 > 3.3$$

The load factor exceeds the minimum factor of safety (as in Appendix J). Therefore, the M3 x 0.5 x 6 Grade 4.8 bolt with threaded insert is suitable.

Appendix Q. Slipping calculation

To determine whether the turbine will slip, a free body diagram is created in Figure 29 below to visualise the acting forces on the body.

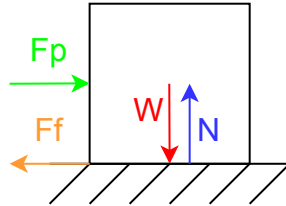


Figure 29: Slipping free body diagram.

Where:

- F_p (N) is the pushing force i.e. the force of the fluid.
- F_f (N) is the frictional force.
- W (N) is the weight of the body.
- N (N) is the normal force.

Assume the mass of the assembly is at worst:

$$m_{\text{assembly}} = 5 \text{ kg}$$

Considering the sum of the vertical acting forces:

$$\begin{aligned} \sum F_y &= N - W = 0 \\ N &= W \\ N &= m_{\text{assembly}} \times g \\ &= 5 \times 9.81 \\ &= 49.05 \text{ N} \rightarrow \end{aligned}$$

Assuming that all air ducts use aluminium and assuming the anti-slip pad is rubber - the static friction coefficient between rubber and aluminium is [37]:

$$\mu_{\text{rubber, aluminium}} = 0.8$$

Considering the sum of the acting horizontal forces for the body to not slip:

$$\sum F_x = F_p - F_f < 0$$

$$F_p < F_f$$

$$F_{\text{fluid, safe}} < \mu_{\text{rubber, aluminium}} \times N$$

$$10 < 0.8 \times 49.05$$

$$10 \text{ N} < 39.24 \text{ N} \text{ which holds true}$$

Since the inequality holds true, the assembly will not slip.

Appendix R. Tipping calculation

To determine whether the turbine will tip, a free body diagram is created in Figure 30 below to visualise the acting forces on the body. The normal force is placed at the tipping corner under the assumption that this is the only point of contact between the body and ground.

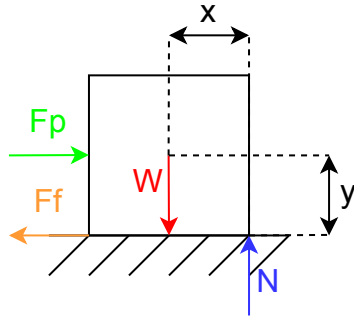


Figure 30: Tipping free body diagram.

Where:

- F_p (N) is the pushing force i.e. the force of the fluid.
- F_f (N) is the frictional force.
- W (N) is the weight of the body.
- N (N) is the normal force.

The position of the centre of mass (with respect to a bottom corner of the assembly) is given by Solidworks:

$$(x, y) = (135, 125) \text{ mm}$$

Consider the moment about the corner of tip for the body to not tip:

$$\begin{aligned} \sum \tau &= \tau_p - \tau_g < 0 \\ \tau_p &< \tau_g \\ y \times F_p &< x \times F_g \\ y \times F_{\text{fluid, safe}} &< x \times m_{\text{assembly}} \times g \\ 0.125 \times 10 &< 0.135 \times 5 \times 9.81 \\ 1.25 \text{ Nm} &< 6.62 \text{ Nm which is true} \end{aligned}$$

Since the inequality holds true, the assembly will not tip.

Appendix S. Three-quarter CAD render

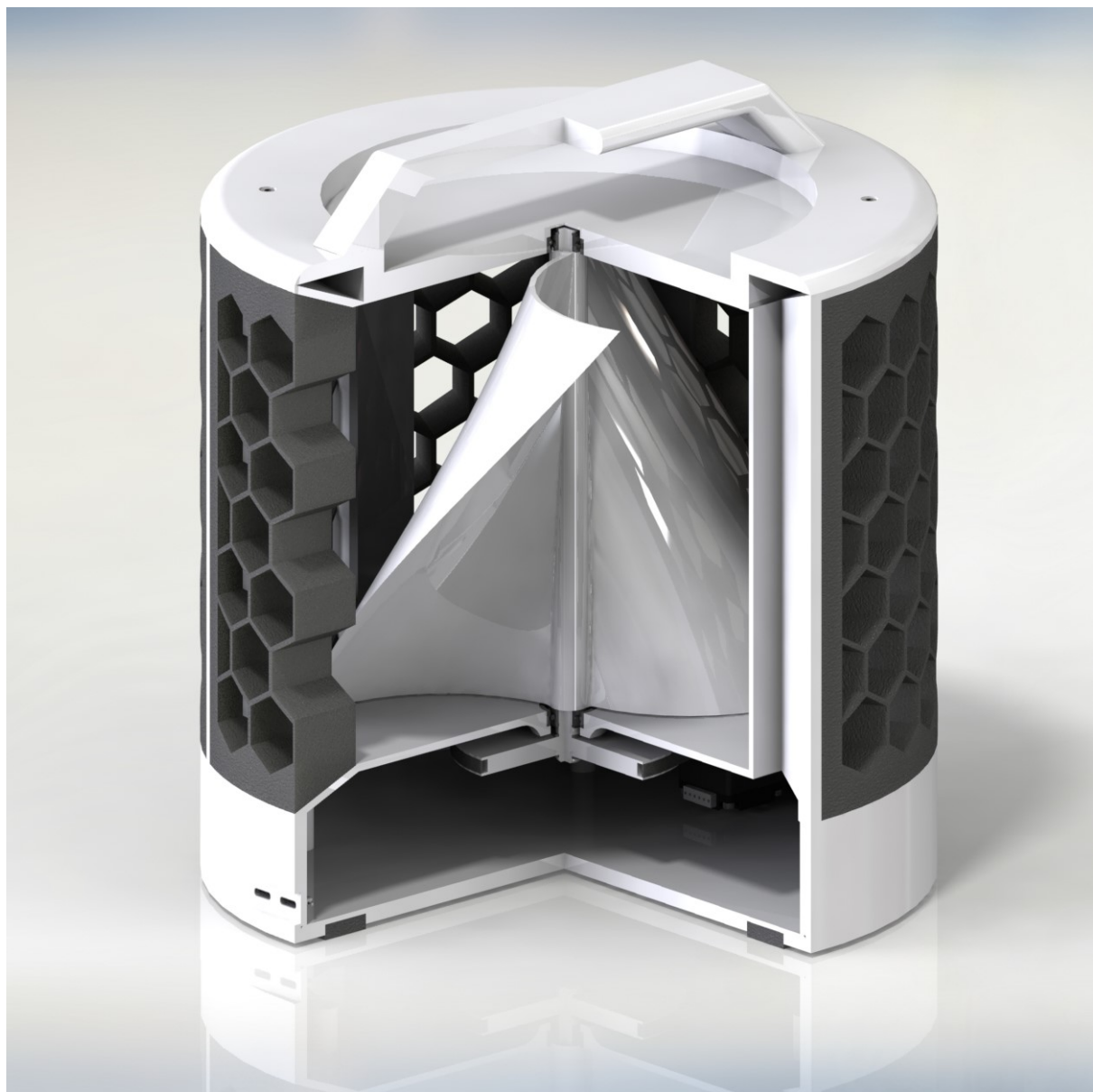


Figure 31: Three-quarter render of the turbine CAD model.

Appendix T. Detailed bill of materials

Table 21: Detailed bill of materials.

PART NO.	DRAW NO.	NAME	DESC.	MTL	QTY	MASS	SRC.	COST
1	3	CASE		ABS PLASTIC	1	887.91		
2	7	SHAFT		ABS PLASTIC	1	19.93		
3	1	BLADE		ABS PLASTIC	1	76.95		
4		FOOT		RUBBER	4	2.40	RS PRO	14.30
5		CIRCLIP	EXTERNAL 10 MM BS3673	STEEL	5	0.41	RS PRO	23.08
6		BEARING	SS61900-2RS	STEEL	3	9.6	RS PRO	8.75
7	9	TOP LID		ABS PLASTIC	1	1546.40		
8	2	BOTTOM LID		ABS PLASTIC	1	1230.41		
9	6	SCREEN		RUBBER	6	141.32		
10		M3 HEX SOCKET BOLT	AS 1420 - M3 X 10-N	STEEL	10	0.13	RS PRO	33.32
11		USB C			4	1.42	CORE ELECTRONICS	4.45
12	5	DRIVING PULLEY		ABS PLASTIC	1	38.70		
13	4	DRIVEN PULLEY		ABS PLASTIC	1	9.69		
14		FEATHER KEY	7 X 3 X 3	STEEL	2	0.45	RS PRO	1.07
15	8	SHORT SHAFT		ABS PLASTIC	1	1.28		
16		BELT		RUBBER	1	1.86	RS PRO	12.51
17		NEMA11			1	111.4	RS PRO	35.05
18	10	NEMA11 MOUNT			1	8.61		
19		M2.5 HEX SOCKET BOLT	AS 1420 - M2.5 X 25-N	STEEL	4	0.16	RS PRO	7.01
24		ARDUINO WIFI SHIELD			1	20	ARDUINO	28.75
25		ARDUINO UNO			1	25	ARDUINO	34.95

Appendix U. Prototype

A prototype of the turbine-generator was 3D-printed to test for demonstration and basic testing. With the prototype shown in Figure 32, the turbine was able to spin under light gusts of wind ($3 - 4 \text{ m/s}$) and cause the motor to turn.



Figure 32: 3D-printed turbine prototype.